12-2017

Simplified model for persistent sliding contact

Adarsh Patil
Purdue University

SIMPLIFIED MODEL FOR PERSISTENT SLIDING CONTACT

A Dissertation

Submitted to the Faculty

of

Purdue University

by

Adarsh Patil

In Partial Fulfillment of the

Requirements for the Degree

of

Master of Science

December 2017

Purdue University

West Lafayette, Indiana

THE PURDUE UNIVERSITY GRADUATE SCHOOL
STATEMENT OF DISSERTATION APPROVAL

Dr. Arun Prakash, Chair

Lyles School of Civil Engineering

Dr. Amit Varma

Lyles School of Civil Engineering

Dr. Ghadir Haikal

Lyles School of Civil Engineering

Approved by:

Dr. Govindaraju Rao

Lyles School of Civil Engineering

To my parents,

Uma and Basavaraj.

ACKNOWLEDGMENTS

I would like to thank my Professor and advisor Dr. Arun Prakash for all the motivation and guidance he has provided me throughout my graduate program. Along with nurturing my knowledge in mechanics, he has helped me in developing professional skills and inculcating work discipline.

I would also like to thank my committee members Dr. Amit Varma and Dr. Ghadir Haikal for providing their valuable time in reviewing my work and providing valuable advice to enrich my work. It was a great honor to work for Indiana Next Generation Manufacturing Competitiveness Center - IN-MaC and Tru-Flex Metal Hose Corporation. I would also thank my friends Rahul Anand and Madhav Sakariya for their assistance in completing this project.

TABLE OF CONTENTS

Page

LIST OF TABLES

LIST OF FIGURES

Figure Page

ABSTRACT

Patil, Adarsh MS, Purdue University, December 2017. Simplified Model for Persistent Sliding Contact. Major Professor: Dr. Arun Prakash. .

Numerous engineering applications involve one or more mechanical components that come into contact with each other during operation. Repetitive motions under contact can lead to fatigue and wear problems in the components. When designing such components, it is important to characterize and quantify the stresses and strains in the contacting elements. This can be achieved by numerical simulation of the process and by using one of the several contact formulations available in most finite element software programs. However, contact is an inherently non-linear problem which is rather challenging even for the best commercial software programs currently available. Often contact simulations are plagued by issues of high computational cost and non-convergence that are highly problem dependent. Further, modeling approaches that work for one scenario do not generalize easily for other problems.

In several applications, one encounters sliding contact that is persistent. In such cases, components always stay in contact during operation but slide with respect to one another within a small range of motion. An example of such an application is the interlock hose where thin strips of sheet metal are coiled together in a way that adjacent coils lock with each other to form a flexible hose. This flexible hose allows a limited amount of motion between adjacent coils by letting the coils slide with respect to each other while always remaining in locked contact.

In this study, a simplified model is developed for applications with persistent sliding contact. The simplified model utilizes slender spring and membrane elements that are stiff in the direction of their orientation but flexible in the transverse direction. The stiff response is used to simulate persistent contact and to prevent gaps or pen-

etration between contacting components and the flexible response is used to create a bi-stable mechanism that mimics sliding between the components. The primary benefit of this approach is that it is far more computationally efficient than conventional approaches for modeling contact with high fidelity. However, given that it is a simplified model, one loses some accuracy in the solution, especially in regions of the model that are actually in contact. Nevertheless, this simplified approach and conventional high-fidelity contact models produce deformations and stresses that are very similar in parts of the model that are away from the immediate region of contact. Several numerical examples are presented to illustrate the simplified model and to compare its performance, both in terms of solution accuracy and computational cost, to conventional high-fidelity contact models.

1. INTRODUCTION

1.1 A brief history of contact mechanics

Contact mechanics is the branch of engineering mechanics which deals with the study of deformation of solids that touch each other at one or more points (see Johnson [1]). Principles of contact mechanics can be applied in areas such as braking systems, tires, bearings, metal-working, electrical contacts, interlocks (discussed in this document) and in many more engineering applications. Applications of contact mechanics further extend into micro and nano-technology as well. Stresses and deflections arising from contact between two bodies have practical applications in hardness testing, wear and impact damage. Hence it is important to understand the effect of contact pressure and tangential tractions on the durability of the components and systems.

The history of contact mechanics dates back to 1882 with Hertz providing his paper on frictionless contact of two elastic bodies of ellipsoidal profile. Important aspects in contact mechanics are the pressures acting perpendicular to the surfaces of the bodies in contact and the frictional stresses acting tangentially between the surfaces. The forces perpendicular(normal) to the interface can be divided into compressive and adhesive forces. In the tangential direction, we usually have frictional forces. Frictional contact mechanics is the study of deformation of bodies in the presence of frictional effects whereas frictionless contact mechanics assumes the absence of such effects.

In this document, we focus on persistent sliding contact between two bodies. Sliding contact is a special type of contact which allows displacement tangential to the contact surface but no relative movement along the normal direction. If there is a difference in the components of the linear velocities of the two points in contact, then

the two surfaces are said to be sliding [2]. In persistent sliding contact problems, the constraints must enforce traction continuity between the two bodies.

1.2 Problems associated with contact mechanics

From a computational point of view, contact problems are challenging. Contact problems are inherently nonlinear since, prior to contact, boundary conditions are given by traction conditions whereas during contact kinematic constraints must be imposed to prevent penetration of one boundary through the other. Physically, all contact surfaces have some roughness associated with them. Thus, when two bodies come into contact, the regions of contact cannot be determined *a priori*. Usually, contact occurs at the peaks of the surface roughness and so the actual area of contact is much smaller than the apparent area of contact between two surfaces. So far, it has proved difficult both, to experimentally measure this real area of contact, and also to theoretically predict it. [3].

In contact simulations, the most important aspects of the solution usually are resolving the area of actual contact and the stress distribution in the contact regions. Depending on the loads, material, boundary conditions, and other factors, surfaces can come into and go out of contact with each other in a largely unpredictable and abrupt manner [4]. Contact problems must also account for friction, and almost all friction models and laws are nonlinear. Even the simple case of non-adhesive, frictionless normal contact problem between two linear elastics solids with randomly rough surfaces is still a controversial scientific issue [5]. This makes convergence in contact simulations very difficult. Furthermore, contact simulations usually are computationally very intensive and often can take hours or days even for relatively small problems.

1.3 Motivation

Interlocks are used in the manufacturing of flexible hoses which are designed for use in post-treatment systems to transfer treated exhaust to the exhaust stack (see Fig. 1.1). Applications of flexible hoses include on and off highway commercial vehicle exhaust systems and use post-treatment system for buses, trucks, tractors, military, construction, forestry, marine, power generation.

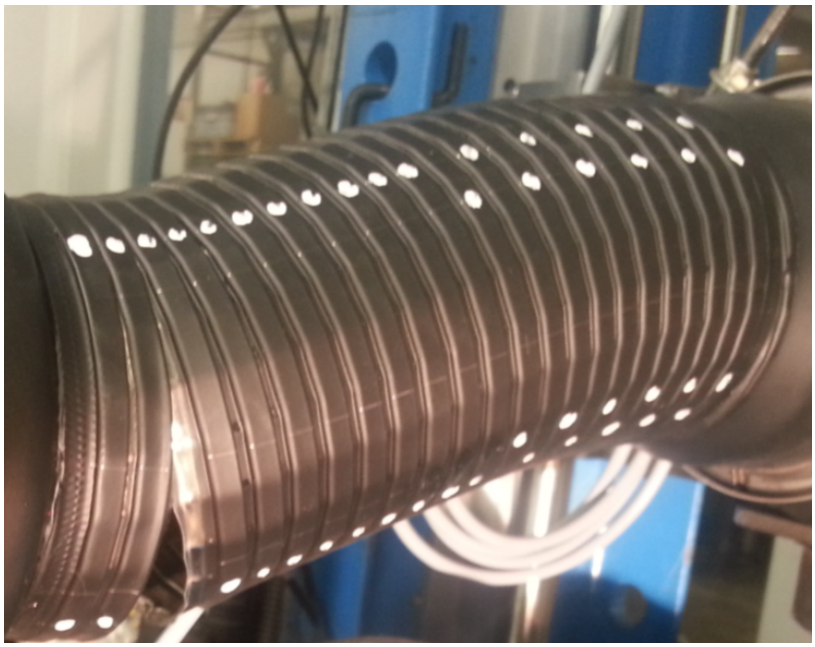

Figure 1.1.: A failed interlock hose

As seen in Figure 1.2, the cross section of the interlock is made of two S-shaped rings attached to each other forming a lock. These cross-sections are revolved and constructed spirally to form a hose as shown in Figure 1.1. Contact arises between the surfaces of the interlock due to the imperfections in the manufacturing process. It is practically impossible to manufacture a completely well polished surface. Hence contact arises due to the surface roughness. As marked in Figure 1.3, 2-ring interlock has four contact surfaces in total. Contact surface 3 and 4 are active in the fully extended and compressed configurations. During the play between the two extreme

positions, contact surfaces 1 and 2 are always active. Due to the presence of contact, there will be high stress concentrations at the region of contact. Analysis of contact stresses becomes a important part in predicting the durability, type of failure of interlocks.

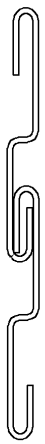

Figure 1.2.: Sectional view of strips of sheet metal forming an interlock

Contact simulations of these interlocks, even for a much simplified geometry of a 2-ring interlock with only one active contact surface, prove to be computationally very expensive. Convergence with two active contact surfaces even for a 2-ring interlock has been found to be very difficult. The non-linearities and computational cost of solving a full multi-ring interlock with all active contact surfaces is practically impossible. Hence there is a strong need to develop a simplified model(without contact) which predicts the approximate contact stresses.

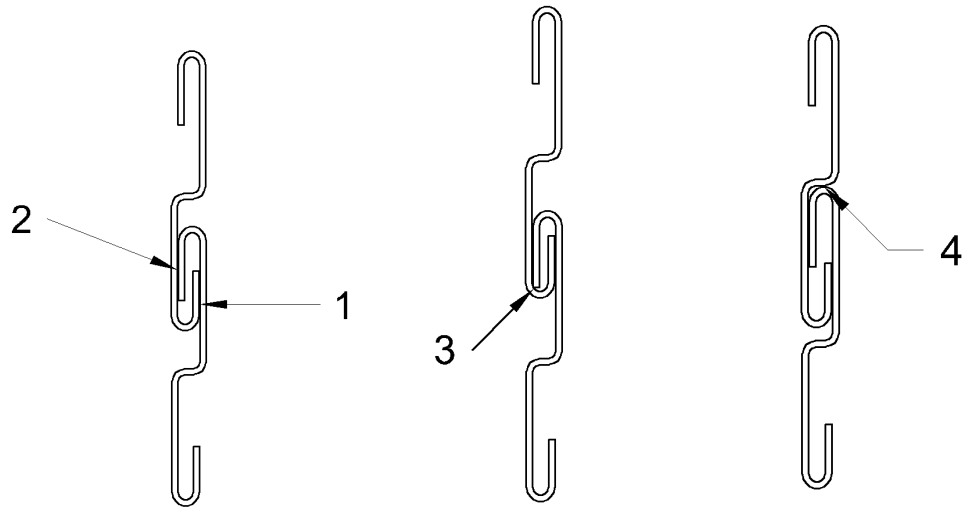

(a) Interlock play (b) Extended state (c) Compressed state

Figure 1.3.: Contact pairs in interlock

1.4 Problem statement

The primary objective of this research is to formulate a simplified model for persistent sliding contact to achieve fast convergence and reduce simulation run time for problems involving sliding contact. The simplified models replace the problem of searching and resolving contact along sliding surfaces with flexible bi-stable mechanisms that mimic the underlying behavior. The parameters of the simplified models are calibrated to reproduce deformation and stresses obtained from pure contact models. Finally, the performance of these simplified models is compared to conventional high-fidelity contact models, both in terms of solution accuracy and computational cost using several numerical examples.

1.5 Approach

Two approaches have been proposed to develop the simplified contact model. The first uses spring elements in a cross pattern and is suitable for primarily two-dimensional problems. The other approach uses membrane elements between surfaces in three-dimensions. Both the approaches use the concept of bi-stable configurations of the spring and membrane elements to mimic the limits of sliding motion. The orientation of the springs in the cross pattern and the membrane elements is chosen such that these simplified contact devices are very stiff in the direction of normal contact and very flexible in the direction of tangential contact.

The stiffness, geometrical dimensions, and the material properties of the spring and membrane elements affect the accuracy of the simplified contact models. For both approaches, multiple combinations of these parameters were run to find their optimal values. Benchmark problems in persistent sliding contact are used to understand the behavior of these simplified models which approximately depict the interlock behavior. Results from the simplified models are compared to those from pure contact models. Simplified contact models for a 2-ring interlock hose were developed compared to pure contact models.

2. BACKGROUND

2.1 Mathematical Formulation

As stated in Chapter 1, Hertz was the first to provide solutions to contact problems and hence traditional mechanics of contact problems is affiliated with Hertz. Mainly Hertz produced simple solutions for elastic contact problems without adhesive forces. Hertzian contact stress describes the stress near the contact area of the two bodies in contact.

Non-adhesive contact assumes that there is no tension force within the contact area, i.e., no adhesive force is required to separate the contacting bodies. When two elastic bodies are in contact, the area of contact between the two bodies and depth of indentation are calculated using this theory of contact mechanics. The contact theory developed by Hertz is used in numerous practical situations of which main five cases are listed below.

1. Case where a spherical body is in contact with an elastic half space.
2. Two spherical bodies in contact
3. Case where two cylindrical bodies with parallel axis are in contact
4. Case where a rigid cylinder is in contact with an elastic half-space
5. Case of a rigid conical indenter in contact with an elastic half space

The contact pressure profile $p(r)$, as described by Hertzian theory, is given by

$$p(r) = p_0\sqrt{1-(r/a)^2}, \qquad r < a \tag{2.1}$$

where p_0 is the peak contact pressure, r is measured from the mid point of contact area, and a is the distance between the mid point and end point of contact area as

shown in Figure 2.1. Equation 2.1 describes the depression produced on the surface of one of the bodies in contact as a parabola. The basic equations in Hertz contact theory are provided below along with the self explanatory diagrams.

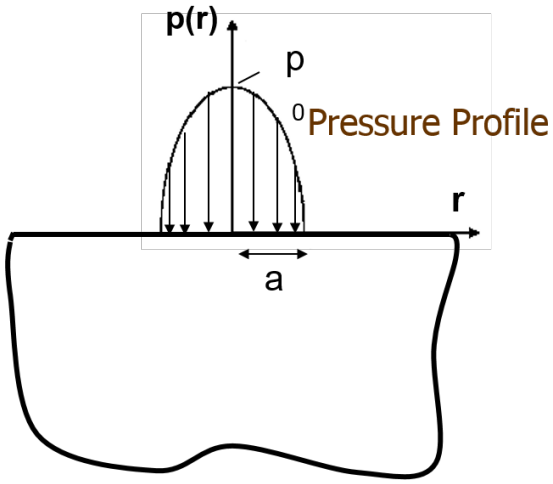

Figure 2.1.: Hertz contact (Source - [6])

Depth at center δ is given by

$$\delta = \frac{(1-\nu^2)\pi}{2E} p_o a \tag{2.2}$$

where ν indicates Poisson's ratio and E indicates Young's modulus. Curvature $\frac{1}{R}$ is given by

$$\frac{1}{R} = \frac{(1-\nu^2)\pi p_o}{2Ea} \tag{2.3}$$

Resultant force P is given by

$$P = \int_0^a p(r) 2\pi r dr = \frac{2}{3}\pi a^2 p_o \tag{2.4}$$

Later, multi-asperity models were developed. [7]. The basic assumptions made in developing these models include neglecting bulk deformation, considering the deformations produced in the contacting bodies to be linearly elastic and isotropic. One such important model is Greenwood and Williamson model. As per this this model, when the asperity heights are distributed as per Gaussian theory,the area of contact

is approximated to be varying linearly in the normal force, elastic deformation is consistent with the Coulomb friction. Figure 2.2 describes the variation of mean real pressure with load. The real pressure changes by a only a factor of 2 when the load undergoes a change by a factor of 10^5.

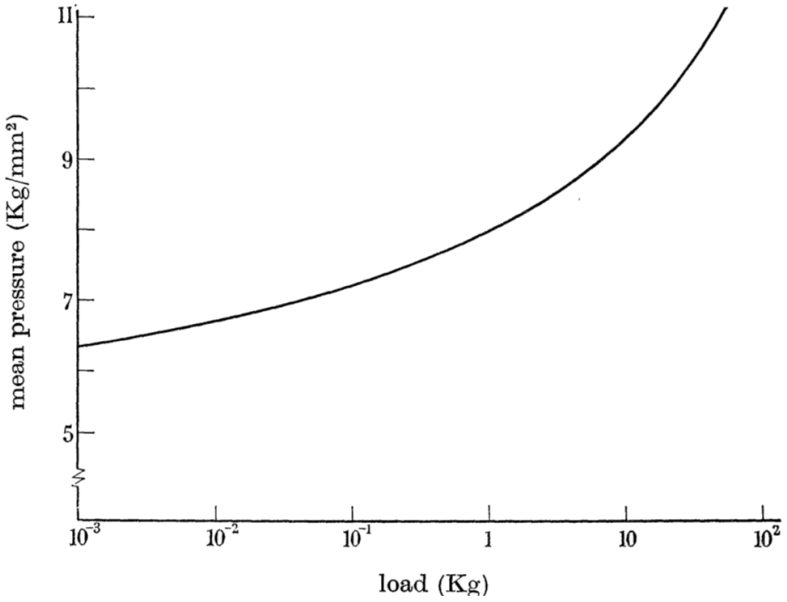

Figure 2.2.: Greenwood and Williamson model (Source - [6])

Several modifications were made to Greenwood and Williamson model importantly incorporating plastic deformation and adhesion. When adhesion is considered, Van der Waals forces play an important role. These forces are characterized by surface energy (γ) and the work of adhesion ($\triangle\gamma$). The work of adhesion ($\triangle\gamma$) when two bodies A and B are in contact is given by

$$\triangle\gamma = \gamma_A + \gamma_B - \gamma_{AB} \tag{2.5}$$

where γ_A is the surface energy of body A, γ_B is the surface energy of body B and γ_{AB} is the surface energy at the interface between bodies A and B.

Several models were proposed for adhesive contact. A brief note on the models is included in this paper.

2.1.1 Bradley model of rigid contact

When two bodies are in contact, the attractive interaction forces between the bodies produces some elastic deformations. These deformations are neglected in Bradley's model of rigid contact. It is a pure Vander Waals model. [8]. It is considered between two rigid spheres as shown in Figure 2.3.

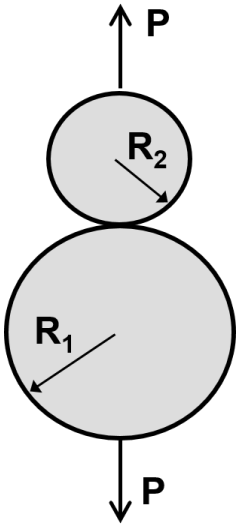

Figure 2.3.: Bradley model (Source - [6])

The force $P_{pull-off}$ required to overcome the adhesion is given by

$$\frac{1}{R} = \frac{1}{R_1} + \frac{1}{R_2}, \quad P_{pull-off} = 2\pi \triangle \gamma R \tag{2.6}$$

the radius of sphere 1 is given by R_1 and the radius of sphere 2 is given by R_2 and the work of adhesion between the two bodies is given by $\triangle\gamma$.

2.1.2 Johnson-Kendall-Roberts (JKR) model of elastic contact

JKR model includes the effect of elastic deformation. Unlike the Bradley model, the JKR model includes the effect due to the forces arising due to the inter facial attraction between the bodies. In fact the area of contact, the forces due to inter facial

attraction and the elastic material properties of the bodies in contact are correlated by this theory. The effect due to adhesive forces which are only assumed in the region of contact is considered as surface energy only but the adhesive stresses are neglected in the separation zone. Stresses tend to infinity around the contact area and within the region of contact, the stresses become compressive in nature at the center and tensile in nature at the ends.

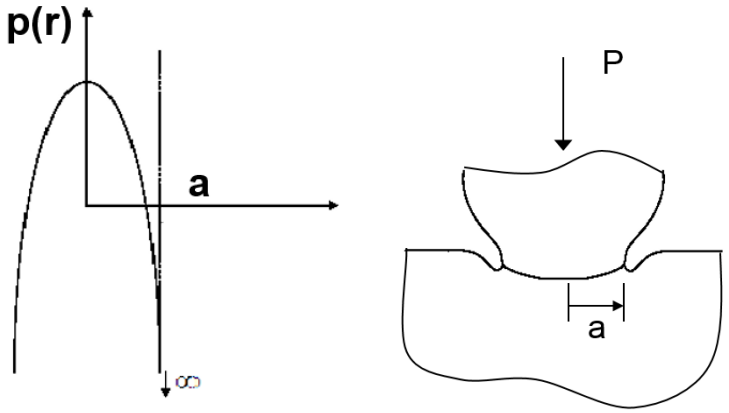

(a) Graph (b) Physical arrangement

Figure 2.4.: JKR model (Source - [6])

The force $P_{pull-off}$ required to overcome the adhesion is given by

$$P_{pull-off} = 1.5\pi\triangle\gamma R \tag{2.7}$$

2.1.3 Derjaguin-Muller-Toporov (DMT) model of elastic contact.

The DMT model assumes The forces due to attractive interaction between the two contacting bodies are considered in DMT model. In addition to JKR model, DMT model also considers the effect of these forces outside the area of contact in addition to the contact profile as in Hertzian contact. Therefore the stresses remain tensile even outside the region of contact but inside they still follow Hertzian profile. [9]

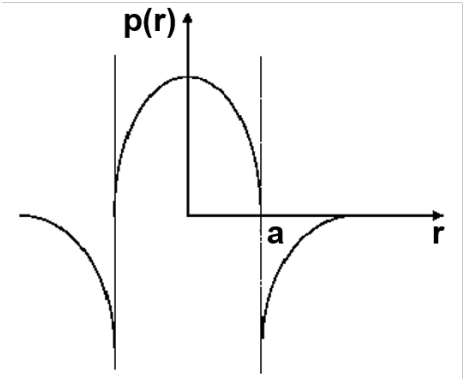

Figure 2.5.: DMT model (Source - [6])

The force $P_{pull-off}$ required to overcome the adhesion is given by

$$P_{pull-off} = 2\pi \triangle \gamma R \tag{2.8}$$

2.1.4 Maugis-Dugdale model of elastic contact

This model modifies the limitations of JKR and DMT model. In 1977, Tabor introduced the non-dimensional parameter called as Tabor parameter. This theory is developed by including the attraction forces due to interaction as described by Lennard-Jones between the two contacting bodies outside the region of contact and a modified JKR theory inside the contact region. Thus, the resulting MaugisDugdale model spans the ranges between the JKR and DMT regions over the range of Tabor parameter. [10].

With the development and need to solve contact problems regularly in engineering practice, achieving contact solutions using boundary value problems came into use. As mentioned in [1], two conditions must be satisfied for using this method. The significant dimensions of the area of contact between the contacting bodies must be small in comparison with

1. The dimensions of the bodies in contact

2. The relative curvature radius of the contacting surfaces

Over the last two decades, a major development towards solving contact problems by mathematical programming has been introduced. There has been much research in using Finite Element techniques in solving contact problems. In these techniques, the potential energy is minimized with constraints applied to solve contact problems. Mathematical programming (linear/quadratic methods) is used to formulate this minimization problem.

2.2 Governing equations and constraints in contact mechanics

The important factor in contact problems is there is the two contacting bodies do not undergo penetration with respect to each other. Not all the points on the contacting surfaces will be in contact. Any point on the contact surface will either be in contact or not in contact. Therefore the gap(g_N, where 'N' indicates the normal direction) between points on the two bodies becomes an important factor. The formulation of these constraint equations is done at the region of contact Another important factor is the contact pressure(p_N). Contact pressure is present only if there is contact between the points on the two bodies. The condition of no contact between the bodies is given by

$$g_N > 0, \quad p_N = 0 \tag{2.9}$$

and the condition of contact between the two bodies is given by

$$g_N = 0, \quad p_N > 0 \tag{2.10}$$

$$g_N p_N = 0 \tag{2.11}$$

Combining Equation 2.9, Equation 2.10 and Equation 2.11 forms the basis for treating contact with frictionless condition. This set of equations is called as Hertz–Signorini-Moreau condition.

When the contacting bodies have linearly elastic material properties, a unique solution can be obtained including these inequalities. Fichera (1964, 1972) [11]. Since then there has been much advancement for the other categories of contact problems.

[12]. Also, it should be noted that these inequalities show the tendency of contact stresses towards zero as we move to the end of contact region. Johnson observed this while studying the asymptotic fields at the region where the contact is ending.

Additional conditions will be introduced if there is friction between the contacting bodies. Friction adds to the nonlinearity of the problem and complicates the proof of existence and uniqueness. Any point in contact can either be in stick or slip conditions. Stick is a state where there is no tangential movement of the points in contact and slip is a state where a point in contact moves in the tangential direction. Therefore the relative displacement between the two points in contact(g_T), where 'T' indicates the tangential direction defines the stick or slip states. Stick state is represented by

$$g_T = 0 \tag{2.12}$$

Slip state is represented by

$$g_T \neq 0 \tag{2.13}$$

These are the basic relations representing contact. More complex functions can be derived to represent contact and different parameters but those are not discussed here. Further equations related to sliding contact are discussed briefly in the following sections.

As quoted in [13] the Coulomb law states that "The contacting surfaces start to move relative to each other once the tangential forces (t_T) exceed a minimum threshold." The case where there is relative tangential movement between the contacting surfaces is known as *sliding*. This can be expressed mathematically as

$$t_T = -\mu \mid p_N \mid \frac{\dot{g_T}}{\parallel \dot{g_T} \parallel} \quad if \quad \parallel t_T \parallel > \mu \mid p_N \mid \tag{2.14}$$

where μ denotes the sliding friction coefficient, $\dot{g_T}$ denotes the relative sliding velocity, p_N is the normal component of contact pressure. The calculated frictional stress ($\boldsymbol{f_s}$) in sliding using Coulomb's law is very high and hence there some limitations. Therefore, a threshold value is developed in most practical cases to limit this frictional stress.

$$\boldsymbol{f_s}(t_T) = \| \ t_T \ \| - h \leq 0, \quad h = min(\mu \mid p_N \mid, Y_o) \tag{2.15}$$

Or,

$$h = \beta Y_o, \quad \beta = \frac{A_r}{A_a} \tag{2.16}$$

where, material elastic limit is described a constitutive parameter Y_o A_r and A_a are the real and nominal area of contact of the contact surface. The amount of flatten of the asperities according to the normal component of contact pressure is given by the factor β. Equation 2.14, Equation 2.15and Equation 2.16 are collectively taken from Coulomb-Orowan law [14] and Shaw law. But the Shaw law is more convenient for numerical purposes as it provides a smooth relation between tangential stress and normal component of contact pressure. In addition to these depending on the tangential stress and the normal component of contact pressure, there are few more non-linear relations which provide a smoother transition. The set of equations performing this can be obtained from [15], [16] or [17]. Furthermore, in several practical cases, the variation of coefficient of friction μ with the changing contact area is considered.

$$\mu = \mu(J) \tag{2.17}$$

where, J is the Jacobian in transforming the area elements. As mentioned in [18], Coulomb's friction law can be described by the relation

$$da = J \, dA, \quad t_T = -\mu(J) \mid p_N \mid \frac{\dot{g_T}}{\| \ \dot{g_T} \ \|} \tag{2.18}$$

where, $\dot{g_T}$ is the time derivative of g_T

$$\dot{g_T} = \frac{\partial g_T}{\partial t}(\boldsymbol{X}, t) \tag{2.19}$$

The slip function can be explained by developing a super ellipse to simplify the notations. This was developed by Mroz and Stupkiewicz.

$$\boldsymbol{f_s}(p_N, \boldsymbol{t_{T_x}}, \boldsymbol{t_{T_y}}) = (\mid \frac{\boldsymbol{t_{T_x}}}{\mu_x} \mid^n + \mid \frac{\boldsymbol{t_{T_y}}}{\mu_y} \mid^n)^{\frac{1}{n}} - p_N \leq 0 \tag{2.20}$$

where the tangential stress in the x-direction is given by $\boldsymbol{t_{T_x}}$ and by $\boldsymbol{t_{T_y}}$ in the y-direction. The elliptical form is characterized by a parameter n. which can found in [19]. Another technique of developing contact equations is computational homogenization which is achieved through numerical simulation. A Representative Volume Element (RVE) is developed to include the real area of contact. It involves several computational simulations to achieve a statistically representative equation.

A major advancement in the recent decades in solving contact problems is by formulating boundary value problems. The resulting boundary value problems which are non-linear in nature are analyzed and solved by a technique known as Finite Element method. Since these non-linearities bring complexity into the problem, weak forms have to be developed to solve them.

Derivation of equations is in itself is a whole chapter. So, a brief note on the important equations is discussed in this paper.

The equations used in linear elasticity are as follows., the state of equilibrium is described by

$$\text{Div}\,\boldsymbol{\sigma} + \boldsymbol{f} = \boldsymbol{0}, \quad \boldsymbol{\epsilon}(\boldsymbol{u}) = \frac{1}{2}(\nabla \boldsymbol{u} + \nabla^T \boldsymbol{u}), \quad \boldsymbol{\sigma}(\boldsymbol{u}) = \mathcal{C}\boldsymbol{\epsilon}(\boldsymbol{u}) \tag{2.21}$$

where $\boldsymbol{\sigma}$ denotes stress tensor, $\boldsymbol{f}$ the body forces, $\boldsymbol{\epsilon}$ the strain field, $\boldsymbol{u}$ is the displacement field, $\mathcal{C}$ is used to denote the elasticity tensor. The Dirichlet conditions which are the boundary conditions imposed on the displacement are given by

$$\boldsymbol{u} = 0 \quad on \quad \tau_{\boldsymbol{u}} \tag{2.22}$$

The Neumann conditions which are the boundary conditions imposed on tractions are given by

$$\boldsymbol{\sigma n} = \bar{\boldsymbol{t}} \quad on \quad \tau_{\boldsymbol{\sigma}} \tag{2.23}$$

where $\boldsymbol{n}$ is the outward normal from the surface and $\bar{\boldsymbol{t}}$ is the imposed traction on $\tau_{\boldsymbol{\sigma}}$. When contact is present, the following conditions apply,

$$u_N - g \leq 0, \quad p_N \leq 0 \quad on \quad \tau_c, \quad (u_N - g)p_N = 0 \tag{2.24}$$

where u_N is the normal component of the displacement field and p_N is the contact pressure. This is Signorini's problem which can be found in [11].

$$u_N = \boldsymbol{u}.\boldsymbol{n} \quad and \quad p_N = \boldsymbol{t}.\boldsymbol{n} \tag{2.25}$$

In a space V, where V denotes the vector valued real functions [20], the virtual displacement $\boldsymbol{v}$ satisfies the condition

$$\boldsymbol{v} = 0 \quad on \quad \tau_{\boldsymbol{u}} \tag{2.26}$$

The contact condition

$$\boldsymbol{v}_N - g \leq 0 \quad \forall\, \boldsymbol{v} \in V \quad with \quad v_N = \boldsymbol{v}.\boldsymbol{n} \tag{2.27}$$

Assuming $\boldsymbol{u}$ to be the solution for Signorini's problem, weak form to Equation 2.27 can be stated as

$$\int_B \boldsymbol{\sigma}.\epsilon(\boldsymbol{u}-\boldsymbol{v})dV = \int_B \overline{\boldsymbol{f}}.(\boldsymbol{u}-\boldsymbol{v})dV + \int_{\tau_{\boldsymbol{\sigma}}} \bar{\boldsymbol{t}}.(\boldsymbol{u}-\boldsymbol{v})d\tau + \int_{\tau_c} p_N(\boldsymbol{u})(u_N - v_N)d\tau \tag{2.28}$$

where $\sigma = \sigma(u)$ as stated in Equation 2.21, $\overline{\boldsymbol{f}}$ indicates the body forces and $\bar{\boldsymbol{t}}$ indicates the boundary tractions. The last term of Equation 2.28 can be written as

$$p_N(u_N - v_N) = p_N(u_N - v_N + g - g) = p_N(v_N - g) \geq 0 \tag{2.29}$$

The solution thus defined collectively by Equations 2.25, 2.26, and 2.27 has to fulfill the inequality

$$\int_B \boldsymbol{\sigma}.\epsilon(\boldsymbol{u}-\boldsymbol{v})dV \geq \int_B \overline{\boldsymbol{f}}.(\boldsymbol{u}-\boldsymbol{v}).dV + \int_{\tau_\sigma} \bar{\boldsymbol{t}}.(\boldsymbol{u}-\boldsymbol{v})d\tau \tag{2.30}$$

Thus a variational inequality is attained due to the presence of contact constraints which provides the solution to Signorini's problem. Hence the problems involving contact are nonlinear. This is due to the inequality constraint imposed on the displacement field. Therefore to solve Equation 2.30, complicated algorithms have to be developed. This can also be reformed in a more abstract way which is usually used in theoretical and mathematical steps used in solving contact problems. The

inequality stated in Equation 2.30 is for frictionless contact. When there is friction, the problem becomes even more complicated. There are constraints in the tangential direction in addition to the inequality constraints in the normal direction in case of friction. It is characterized by sudden change of state from stick to slip. This leads to even more mathematical difficulties. A detailed information on variational inequalities mentioned can be found in [12], [21], [22] or [20].

2.3 Discretization

There are a certain methods in which the discretization of the contact surface can be achieved. But discretization of the contact surface using isoparametrization is discussed here. The process involves isoparametric mapping. This connects the surfaces ∂B^1 and ∂B^2 at the contact region.

Isoparametric interpolation is used to discretize the gap function g_N. I is used to denote the nodes present on the surface of the isoparametric elements.

$$\begin{aligned} g_N &= \sum_I N_I(\xi,\eta) g_{NI}, \\ \delta g_N &= \sum_I N_I(\xi,\eta)(\boldsymbol{\eta_I^2} - \boldsymbol{\eta_I^1}) \cdot \boldsymbol{n^1} \\ \Delta g_N &= \sum_I N_I(\xi,\eta)(\boldsymbol{\Delta u_I^2} - \boldsymbol{\Delta u_I^1}) \cdot \boldsymbol{n^1}, \end{aligned} \tag{2.31}$$

where ξ and η are the coordinates.

The discretized surface of body B^1 has a normal vector ($\boldsymbol{n^1}$) which is given by

$$\boldsymbol{n^1} = \frac{\boldsymbol{G_1^1} \times \boldsymbol{G_2^1}}{\| \boldsymbol{G_1^1} \times \boldsymbol{G_2^1} \|} \tag{2.32}$$

where $\boldsymbol{G_\alpha^1}$ are the tangential vectors. These are calculated by differentiating position vector ($\boldsymbol{X_{,\xi}^1}$) partially with respect to the undeformed (initial) configuration, $\boldsymbol{G_\alpha^1} = \boldsymbol{X_{,\xi}^1}$ i.e. with coordinates ξ and η. Therefore the contact normal becomes

$$\boldsymbol{n^1} = \frac{\boldsymbol{X_{,\xi}^1} \times \boldsymbol{X_{,\eta}^1}}{\| \boldsymbol{X_{,\xi}^1} \times \boldsymbol{X_{,\eta}^1} \|} \tag{2.33}$$

The position vector $\boldsymbol{X^1}$ is approximated by

$$\boldsymbol{X^1} = \sum_{I=1}^{m} N_I(\xi,\eta)\boldsymbol{X}_I^1, \tag{2.34}$$

The derivatives $(X_{i,\alpha}^1)$,

$$X_{i,\alpha}^1 = \sum_{I=1}^{m} N_I(\xi,\eta)_{,\alpha} X_{i\ I}^1, \tag{2.35}$$

Evaluating Equation 2.33 leads to

$$\boldsymbol{N}^1(\xi,\eta) = \boldsymbol{X}_{,\xi}^1 \times \boldsymbol{X}_{,\eta}^1 = \begin{Bmatrix} X_{2,\xi}^1 X_{3,\eta}^1 - X_{3,\xi}^1 X_{2,\eta}^1 \\ X_{3,\xi}^1 X_{1,\eta}^1 - X_{1,\xi}^1 X_{3,\eta}^1 \\ X_{1,\xi}^1 X_{2,\eta}^1 - X_{2,\xi}^1 X_{1,\eta}^1 \end{Bmatrix}. \tag{2.36}$$

Introducing the vectors

$$\eta_{c\ I} = \begin{Bmatrix} \eta_I^2 \\ \eta_I^1 \end{Bmatrix}, \quad \boldsymbol{\Delta u}_{c\ I} = \begin{Bmatrix} \boldsymbol{\Delta u}_I^2 \\ \boldsymbol{\Delta u}_I^1 \end{Bmatrix} \quad and \quad \hat{\boldsymbol{N}} = \begin{Bmatrix} \boldsymbol{N}_I^1 \\ -\boldsymbol{N}_I^1 \end{Bmatrix} \tag{2.37}$$

Gap function variation and linearization are obtained

$$\delta g_N = \sum_I \eta_{c\ I}^T [N_I(\xi,\eta)\hat{\boldsymbol{N}}(\xi,\eta)/ \parallel \boldsymbol{N}^1 \parallel]$$

,

$$\Delta g_N = [\sum_I N_I(\xi,\eta)\hat{\boldsymbol{N}}(\xi,\eta)^T/ \parallel \boldsymbol{N}^1 \parallel]\boldsymbol{\Delta u}_{c\ I} \tag{2.38}$$

In addition to Equation 2.38, discretization for Lagrange multipliers and its variation are obtained. N_I and M_K are the shape functions.

$$\lambda_N = \sum_K M_K(\xi,\eta)\lambda_{NK} \quad and \quad \delta\lambda_N = \sum_K M_K(\xi,\eta)\delta\lambda_{NK} \tag{2.39}$$

Equation 2.36 contributes to the contact part of the weak form. The weak form in equilibrium condition is obtained as

$$\int_{\Gamma_c^e} \lambda\delta_N g_N d\Gamma \approx \sum_{I=1}^{n} \boldsymbol{\eta}_{c\ I}^T \boldsymbol{G}_{c\ I}^u \tag{2.40}$$

where,

$$\boldsymbol{G}^u_{c\ I} = \int_{-1}^{+1}\int_{-1}^{+1} \lambda_N(\xi,\eta) N_I(\xi,\eta)\hat{\boldsymbol{N}}(\xi,\eta) d\xi d\eta. \tag{2.41}$$

The area element $d\Gamma = \parallel \boldsymbol{X}^1_{,\xi} \times \boldsymbol{X}^1_{,\eta} \parallel d\xi d\eta = \parallel \boldsymbol{N}^1 \parallel d\xi d\eta$. Γ^e_c is the contact surface. Further the weak form is developed as

$$\int_{\Gamma^e_c} \delta\lambda_N g_N d\Gamma \approx \sum_{I=1}^{n} \delta\lambda_{N\ K} G^{\lambda}_{c\ K} \tag{2.42}$$

where,

$$G^{\lambda}_{c\ K} = \int_{-1}^{+1}\int_{-1}^{+1} M_K(\xi,\eta) g_N(\xi,\eta) \parallel \boldsymbol{N}^1 \parallel d\xi d\eta. \tag{2.43}$$

In matrix form, Equation 2.40 can be expressed as

$$\int_{\Gamma^e_c} \lambda_N \delta g_N d\Gamma \approx \langle \boldsymbol{\eta}^T_{c1}, \cdots, \boldsymbol{\eta}^T_{c1} \rangle \begin{Bmatrix} \boldsymbol{G}^u_{c1} \\ \vdots \\ \boldsymbol{G}^u_{cn} \end{Bmatrix}, \tag{2.44}$$

and Equation 2.42 can be expressed as

$$\int_{\Gamma^e_c} \delta\lambda_N g_N d\Gamma \approx \langle \delta\lambda_{N1}, \cdots, \delta\lambda_{Nm} \rangle \begin{Bmatrix} G^u_{c1} \\ \vdots \\ G^u_{cm} \end{Bmatrix}, \tag{2.45}$$

Linearization of Equation 2.40 and Equation 2.42

$$\int_{\Gamma^e_c} \lambda_N \delta g_N d\Gamma \approx \sum_{I=1}^{n}\sum_{K=1}^{m} \boldsymbol{\eta}^T_{cI} \boldsymbol{C}_{IK} \Delta\lambda_{NK} \tag{2.46}$$

where,

$$\boldsymbol{C}_{IK} = \int_{-1}^{+1}\int_{-1}^{+1} M_K(\xi,\eta) N_I(\xi,\eta)\hat{\boldsymbol{N}}(\xi,\eta) d\xi d\eta. \tag{2.47}$$

and

$$\int_{\Gamma^e_c} \delta\lambda_N g_N d\Gamma \approx \sum_{I=1}^{n}\sum_{K=1}^{m} \delta\lambda_{NK} \boldsymbol{C}_{KI} \boldsymbol{\Delta u}_I \tag{2.48}$$

with $\boldsymbol{C}_{KI} = \boldsymbol{C}_{IK}^T$. The full matrix form of linearization for one contact element,

$$\langle \boldsymbol{\eta}_{c1}^T, \cdots, \boldsymbol{\eta}^T, \delta\lambda_{N1}, \cdots, \delta\lambda_{Nm} \rangle \boldsymbol{K}_e^{LM} \begin{Bmatrix} \boldsymbol{\Delta u}_1 \\ \vdots \\ \boldsymbol{\Delta u}_n \\ \Delta\lambda_{N1} \\ \vdots \\ \Delta\lambda_{Nm} \end{Bmatrix}, \tag{2.49}$$

with stiffness matrix of element ($\boldsymbol{K}_e^{LM}$)

$$\boldsymbol{K}_e^{LM} = \begin{bmatrix} & & & \boldsymbol{C}_{11} & \cdots & \boldsymbol{C}_{1m} \\ & \boldsymbol{0} & & \vdots & \vdots & \vdots \\ & & & \boldsymbol{C}_{11} & \cdots & \boldsymbol{C}_{1m} \\ \boldsymbol{C}_{11}^T & \cdots & \boldsymbol{C}_{n1}^T & & & \\ \vdots & \vdots & \vdots & & \boldsymbol{0} & \\ \boldsymbol{C}_{1m}^T & \cdots & \boldsymbol{C}_{nm}^T & & & \end{bmatrix} \tag{2.50}$$

where m denotes the total nodes used for interpolation, n varies with shape functions.

2.4 Verification

The commercial software program, ANSYS, is used for contact simulations in this study. Two simple problems are analyzed first for understanding the contact capabilities in ANSYS.

2.4.1 Sliding contact between two cubes

In this example, two cubes of different sizes are taken with the smaller cube sliding on top of the larger cube as shown in Figure 2.6. The bottom face (A) of lower cube is fixed, the top face (B) of upper cube is pushed down to bring both the cubes in contact and then the top cube is pushed back and forth to allow sliding between the

cubes. The properties of the cubes, boundary conditions, mesh details and the results are given in Table 2.1. The deformed shapes and equivalent stress plot of the cubes are shown in Figure 2.7.

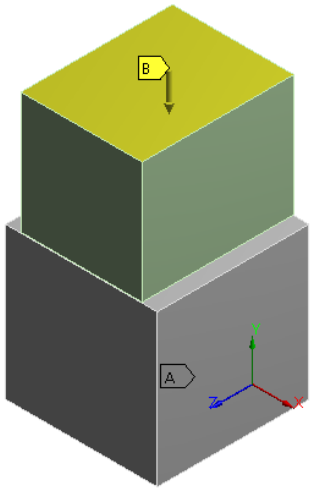

Figure 2.6.: Two cubes in persistent sliding contact

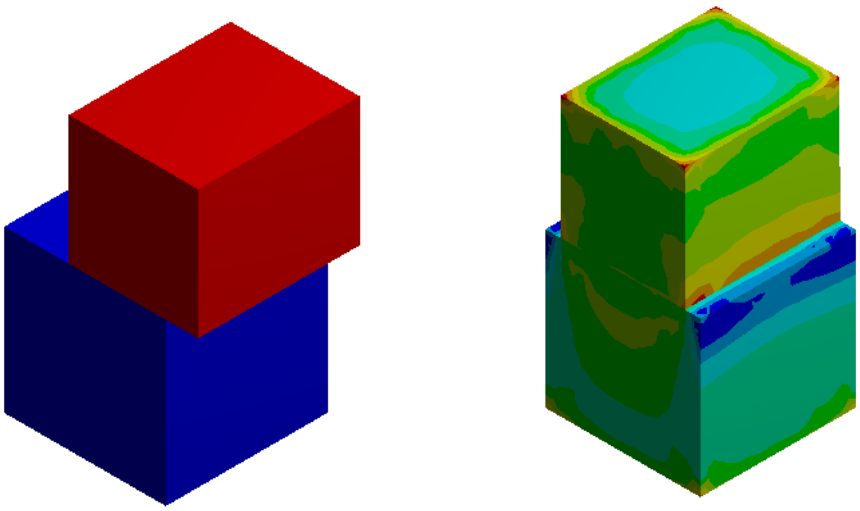

(a) Cube - Deformed shape

(b) Cube - Equivalent stress

Figure 2.7.: Cube results

Table 2.1.: Properties of two-cube contact model

Properties		Lower cube		Upper cube		
	Length X	10 in.		8 in.		
	Length Y	10 in.		8 in.		
	Length Z	10 in.		10 in.		
	Volume	1000 in^3		640 in^3		
Contact	Frictional with friction coefficient 0.1					
Mesh	Method	Tetrahedrons				
	Element Size	1 in.				
	Relevance center	Coarse				
	Behavior	Soft				
	Algorithm	Patch confirming				
	Nodes	21906				
	Elements	14661				
Analysis settings	Number of steps	2				
	Initial sub steps	10				
	Minimum sub steps	10				
	Maximum sub steps	20				
Boundary conditions	Lower Cube- Bottom face is fixed	Upper Cube-Top face displacement				
		Steps	Time(s)	X(in)	Y(in)	Z(in)
		1	0	0	0	0
		1	1	0	-0.06	0
		2	2	3	-0.06	0
Results	Total Deformation (in)	Minimum		Maximum		
		0		0.77		
	Equivalent(Von-Mises) stress(psi)	Minimum		Maximum		
		696.01		29697		
	Directional deformation (X-axis)(in)	Minimum		Maximum		
		-7.15E-5		3		
	Directional deformation (Y-axis)(in)	Minimum		Maximum		
		-0.06		0		
	Shear stress(psi)	Minimum		Maximum		
		-3699.6		12416		

2.4.2 Cantilever beams in contact

Contact conditions in interlock hoses resembles that of contact between two cantilever beams sliding with respect to each other. The resemblance of two cantilever beam model to interlock is shown in Figure 2.8 and Figure 2.9. Considering the encircled part and activating the contact surface 1, the corresponding boundary conditions are applied to the two cantilever beams. The physical problem and the setup of the models are described in the following sections.

This model consists of two cantilever beams, one on top of other with initial overlap as shown in Figure 2.9. Vertical and horizontal displacements are given to the far end faces of the beams. The displacements are provided in opposite 'y' directions as shown in Figure 2.9 to the faces 'A' and 'B'. The details of the model are provided in Table 2.2. The deformation and equivalent stress plots are shown in Figure 2.10.

Figure 2.8.: Verification of contact capabilities in ANSYS

Table 2.2.: Properties of two-cantilever beam contact model

Properties		Lower beam		Upper beam
	Length X	120 in.		120 in.
	Length Y	10 in.		10 in.
	Length Z	10 in.		10 in.
	Material	Structural steel		
Contact	Frictionless			
Mesh	Method	Tetrahedrons		
	Element Size	4 in.		
	Relevance center	Coarse		
	Behavior	Soft		
	Algorithm	Patch confirming		
	Nodes	5562		
	Elements	3266		
Analysis settings	Number of steps	60		
	Initial sub steps	Were varied for different steps		
	Minimum sub steps	Were varied for different steps		
	Maximum sub steps	Were varied for different steps		
Boundary conditions	Displacement(in)	X	Y	Z
	Upper beam	0	-59.5	0
	Lower beam	0	59.5	0
Results	Equivalent(Von-Mises) stress(psi)	Minimum		Maximum
		3771.8		2.045E+6
	Directional deformation (X-axis)(in)	Minimum		Maximum
		-24.326		24.33
	Directional deformation (Y-axis)(in)	Minimum		Maximum
		-0.5		0.5
	Shear stress(psi)	Minimum		Maximum
		-5.356E+5		5.356E+5

Figure 2.9.: Two cantilever beams in sliding contact: boundary conditions

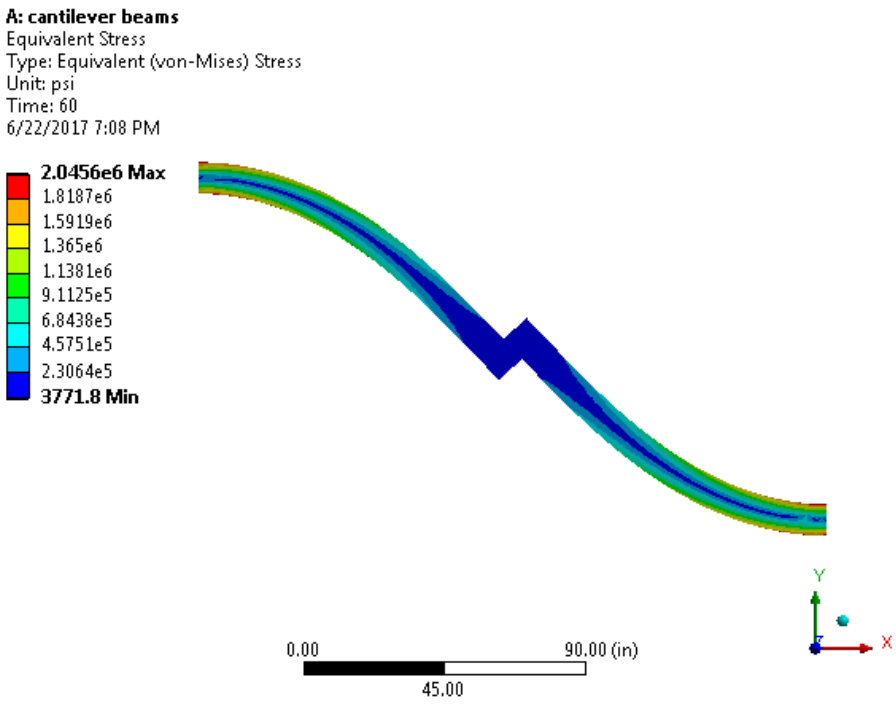

Figure 2.10.: Two cantilever beams in sliding contact: Von-mises Stress and deformation results

Having verified certain basic contact capabilities in ANSYS using the simple examples described in this section, we focus next on developing simplified models for persistent sliding contact in the next chapter.

3. SIMPLIFIED MODELS FOR PERSISTENT SLIDING CONTACT

Since sliding contact is a highly non-linear problem, it is difficult to simulate such problems even the best available software programs, such as ANSYS. In this research, we come up with a simplified model for persistent sliding contact by avoiding the searching and resolution of contact (as is done in conventional contact formulations), and instead simulating the effect of contact using flexible bi-stable devices. Two different approaches are proposed (for 2D and 3D problems) to develop these reduced simplified models to eliminate contact and speed up the computation. The basic idea is to avoid penetration (or gaps) between two sliding bodies (without explicitly modeling contact), but to allow relative movement between them. Comparisons between the actual contact and simplified contact models are made using stress and deformation plots and quantitative stress profiles.

3.1 Bi-stable spring mechanism for 2D persistent sliding contact

For two-dimensional problems, spring elements are used in a cross-pattern to construct a 'fictitious contact device' that has two stable configurations. When two springs are arranged as shown in Figure 3.1, there is high resistance to the vertical motion of node A, but very small resistance to its horizontal motion. When a horizontal load is applied at point A as shown in Figure 3.1, the springs flip with relative ease and reach the other stable configuration.

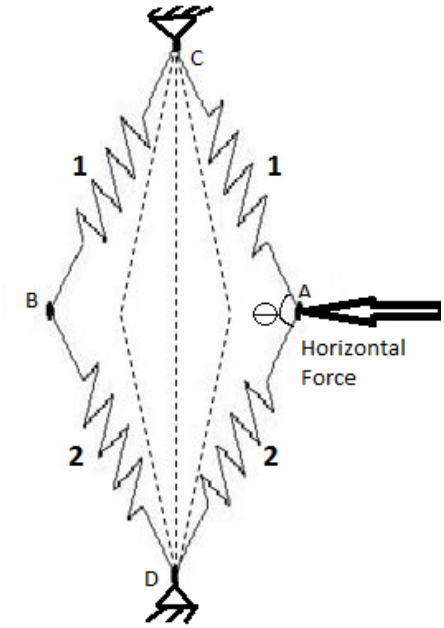

Figure 3.1.: Bi-stable spring mechanism

3.1.1 Behavior of the bi-stable spring mechanism

Consider Figure 3.1, the springs are arranged in such manner as to achieve an obtuse angle θ between them. When a horizontal force is applied at point A, the springs follow a minimum energy path and flip to reach the other stable (stress free) configuration. The maximum stress state of the springs is reached when the springs are at the middle of the path i.e. when the angle between the springs is 180°. Therefore this mechanism of two stress free states is called as bi-stable spring mechanism.

This concept is used to replicate the behavior of persistent sliding contact between two bodies. Consider a situation where there is persistent sliding between two bodies in the horizontal direction and resistance to vertical penetration due to presence of contact. The arrangement of springs as in Figure 3.1 allows movement in the horizontal direction and provides resistance to the vertical motion. This is explained

through graphs by plotting force-deformation curves for forces in the x and y directions. Between the two stress free states, we need relatively much smaller forces in the x-direction and obtain comparatively higher forces in the y-direction. A simulation was run by creating a physical model as in Figure 3.1. Initially point A was pulled in the positive x-direction and pushed towards other flipped state and further.

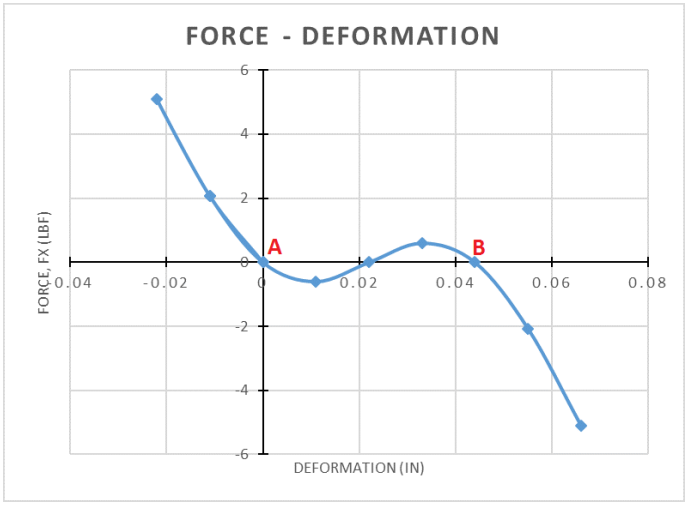

(a) Force in x-direction

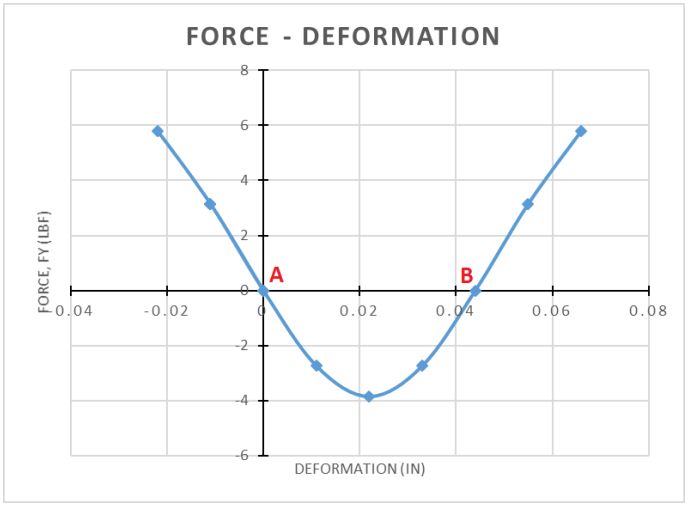

(b) Force in y-direction

Figure 3.2.: Spring Force-deformation plot

Consider Figure 3.2(a), the two stable configurations are achieved at point A and point B. It is evident that there is lesser horizontal force needed to move between points A and B and this can be used to model any frictional resistance to sliding contact, while the resistance to move beyond points A and B increases rapidly which represents the limits of the sliding movement. Therefore the distance between the points A and B is the amount of sliding allowed. The amount of force needed and the amount of sliding permitted can be altered by varying the geometry and stiffness of the springs as needed. From Figure 3.2(b), between points A and B, one may also note that the vertical force is four times higher which represents resistance to penetration in normal contact. Beyond points A and B the direction of force changes but that is not our area of interest. This mechanism is used to develop a simplified contact model for two-dimensional problems as discussed next.

3.1.2 Sliding contact between two cantilever beams in 2D

In this section, the bi-stable spring mechanism is used to construct a simplified contact device for the benchmark problem of two cantilever beams in sliding contact. As shown in Figure 3.3, this system has two cantilever beams with an initial gap of 0.001 in. This system was tested by providing vertical displacements to the far end faces (points A and B) in Figure 3.3 of the beams so that they slide against each other and separate. The objective of this test was to understand the range of vertical displacements the simplified model can model.

Figure 3.3.: Cantilever beams in sliding contact: boundary conditions

The simplified contact model consists of two cross elements which form the supporting structures for two sets of the bi-stable spring mechanism as shown in Figure 3.4. The cross elements are assigned very stiff material properties to restrict their deformation. Springs are connected to the cross elements in way to make them very stiff in the y-direction and allow sliding in the x-direction. The arrangement of cross elements and springs is similar to the one explained earlier in section 3.1.

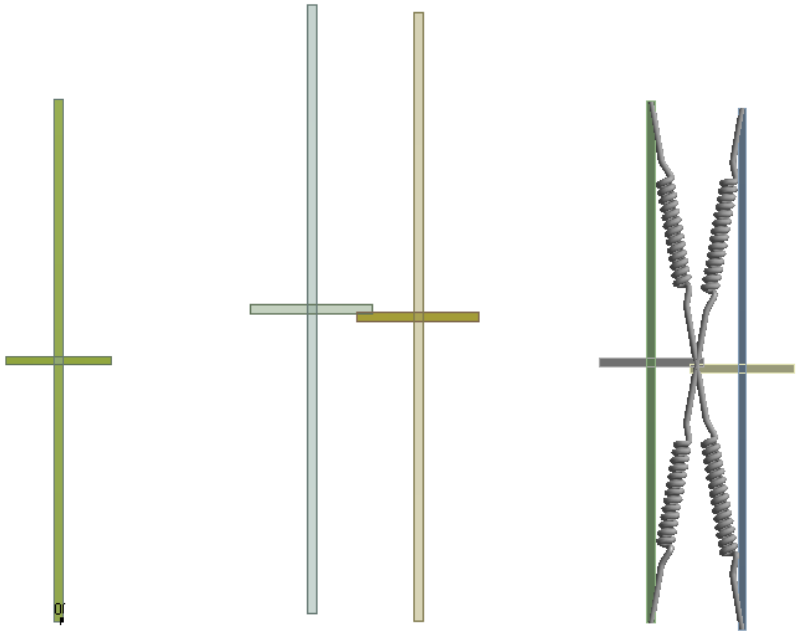

(a) Single cross element (b) Two cross elements (c) Cross elements with bi-stable springs

Figure 3.4.: Simplified contact device: cross elements and bi-stable spring mechanism

The attachment of the simplified contact device to the cantilever beams is shown in Figure 3.5. The horizontal bar of one of the cross elements is attached to the contacting surface of one of the beams to replicate stresses due to contact with the other beam in that region. The horizontal bar of the other cross element is attached to the opposite contacting surface of the other beam. Note that there is a small offset in the vertical position of the two horizontal legs of the cross elements. This offset

enables the attachment of the lower cross element to the bottom (contacting) surface of the top beam and the attachment of the upper cross element to top (contacting) surface of the bottom beam. This type of arrangement achieves the desired sliding contact behavior (while not having to model contact explicitly). The cantilever beams can slide with respect to each other relatively easily in the horizontal direction, while their relative vertical motion is resisted by the bi-stable springs in the cross pattern. Note also, that since the device has two sets of bi-stable springs, there are actually four stress-free stable configurations of the system. Details of the geometry and material properties for the pure contact model are provided in Table 3.1.

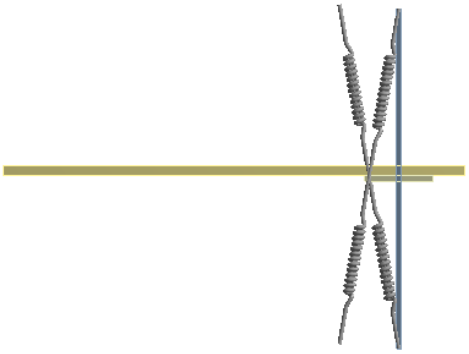

(a) Cross element attached to one beam

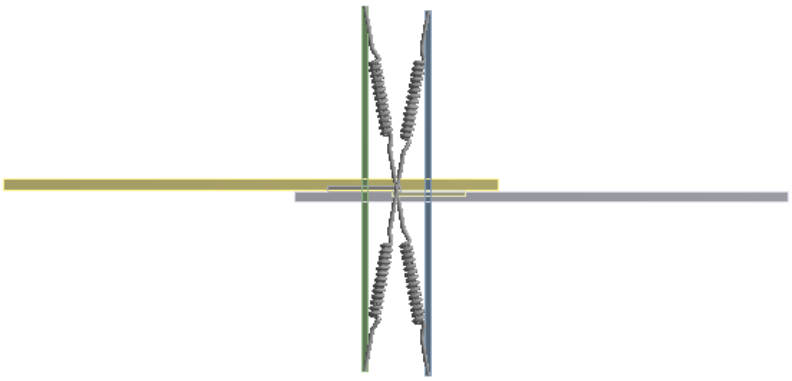

(b) Complete arrangement of the simplified contact device

Figure 3.5.: Simplified contact device attached to two cantilever beams

Table 3.1.: Geometric and material properties of sliding cantilever beams model

Boundary conditions			Lower beam	Upper beam	
	Length X		0.48 in	0.458 in	
	Length Y		0.011 in.	0.011 in.	
	Length Z		0.011 in.	0.011 in.	
Material properties	Material		Structural steel		
	Youngs modulus		2.9E+07 psi		
	Poissons ratio		0.3		
	Behavior		Isotropic elastic		
Contact	Frictionless				
Mesh	Method		Quadrilateral dominant		
	Element size		0.00275 in		
	Nodes		4938		
	Elements		1406		
Analysis settings	Number of steps		38		
	Initial sub steps		20-200		
	Minimum sub steps		20-200		
	Maximum sub steps		500		
Boundary conditions		Displacement	X	Y	Z
	Case i	Edge A	0 in	-0.06 in	0
		Edge B	0 in	0.06 in	0
	Case ii	Edge A	0 in	-0.1in	0
		Edge B	0 in	0.1 in	0
	Case iii	Edge A	0 in	-0.24 in	0
		Edge B	0 in	0.24 in	0

For the simplified contact model, different values for the properties of the spring elements were considered. These are listed in Table 3.2.

Table 3.2.: Cantilever beams 2D - cases considered

Case no.	Spring stiffness (lbf/in)	Stiffness of cross elements/beams	Mesh size(in)	Dimensions of cross elements(in), Horizontal x vertical
1	20	10^1	0.00275	0.0715 x 0.3575
2	20	10^2	0.00275	0.0715 x 0.3575
3	20	10^3	0.00275	0.0715 x 0.3575
4	100	10^1	0.00275	0.0715 x 0.3575
5	100	10^2	0.00275	0.0715 x 0.3575

The results obtained from the five cases above were compared to those from the pure contact model and it was found that values in case 3 matched very well to the pure contact solution. Deformation and Von-Mises stress plots obtained from case 3 of the simplified contact model and the pure contact model are presented in Figure 3.6. It is evident that the deformation and stress response of the simplified contact model is very similar to that of the pure contact model at a fraction of the computational cost. The beams undergo bending in an expected manner and the springs flip facilitating the sliding between the beams. The simple cantilever beam 2D pure contact model with 4938 nodes consumed about 8-hours to simulate whereas the simplified model with even more number of elements due to the addition of cross elements consumed about 30 minutes to converge.

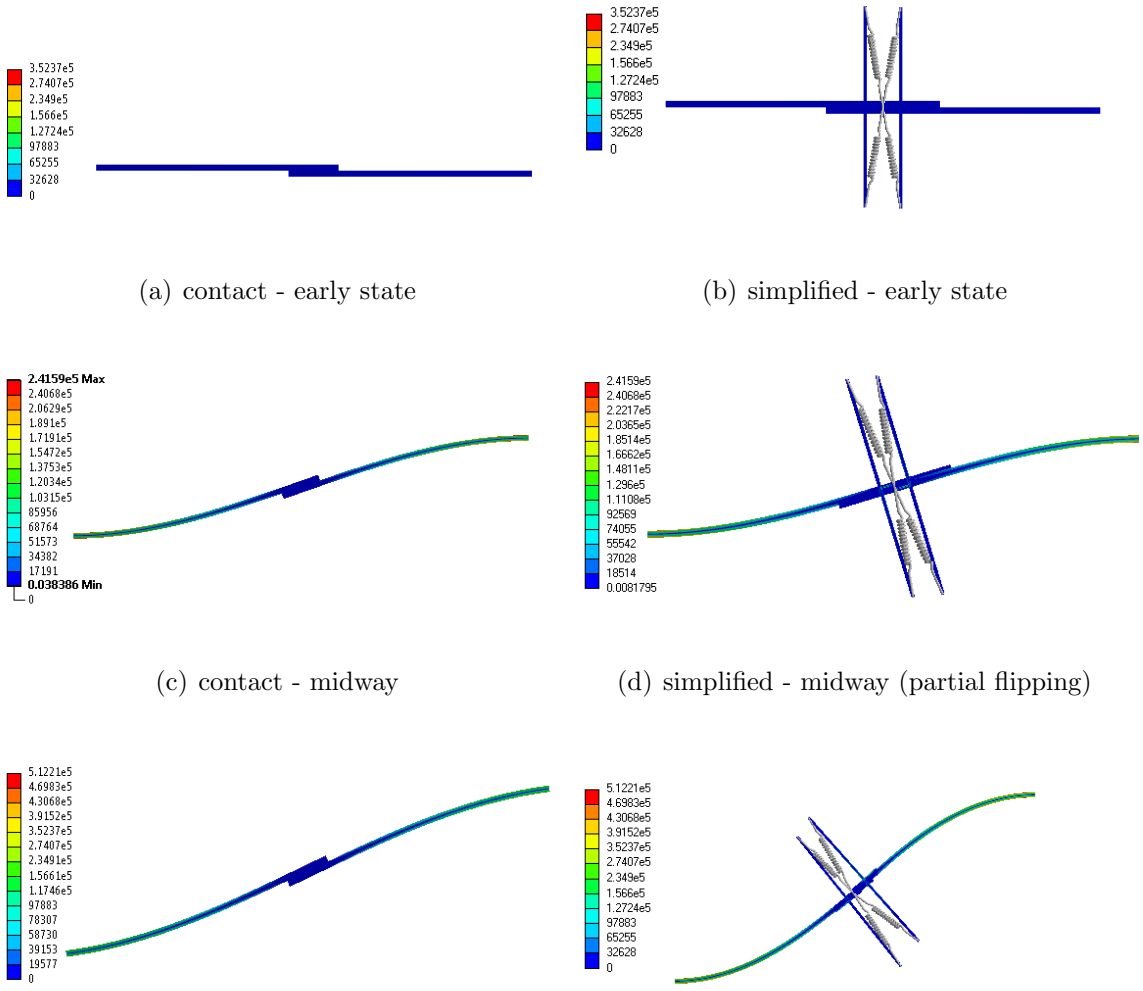

(a) contact - early state

(b) simplified - early state

(c) contact - midway

(d) simplified - midway (partial flipping)

(e) contact - final

(f) simplified - final (total flipped)

Figure 3.6.: Two sliding cantilever beams in 2D: Comparison of deformed shapes for pure contact method and simplified contact method at different stages of loading

A closer comparison of the results from the two models was conducted by developing the contact stress profile along a line of nodes shown in Figure 3.7. Nodes are selected starting from point 'O' and going left by 0.16 in. up to point 'P'. Considering point 'O' as the origin, the minimum principal stress is plot at each of the selected

nodes in Figure 3.8. The stress profile along the contact edge is found to be very similar for the pure contact and case 3 of the simplified contact models.

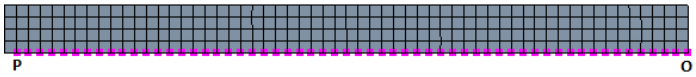

Figure 3.7.: Line of nodes chosen for comparing contact stresses on the upper cantilever beam

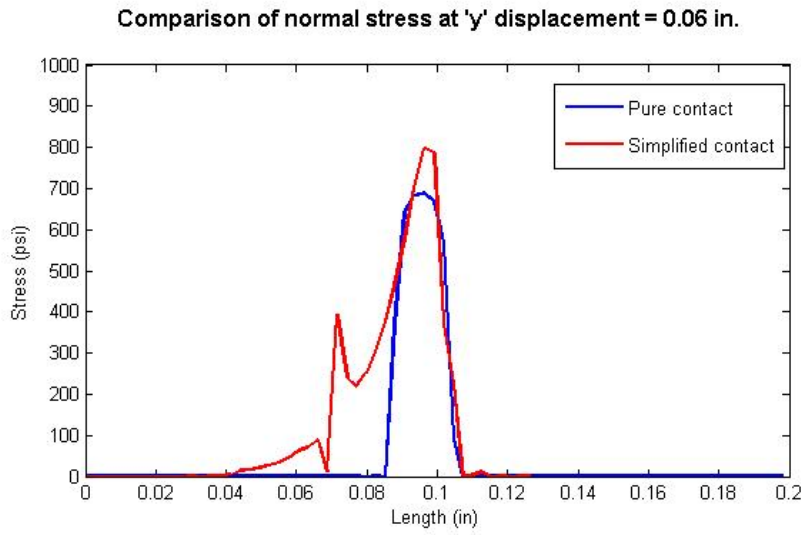

(a) At y-displacement 0.06 in

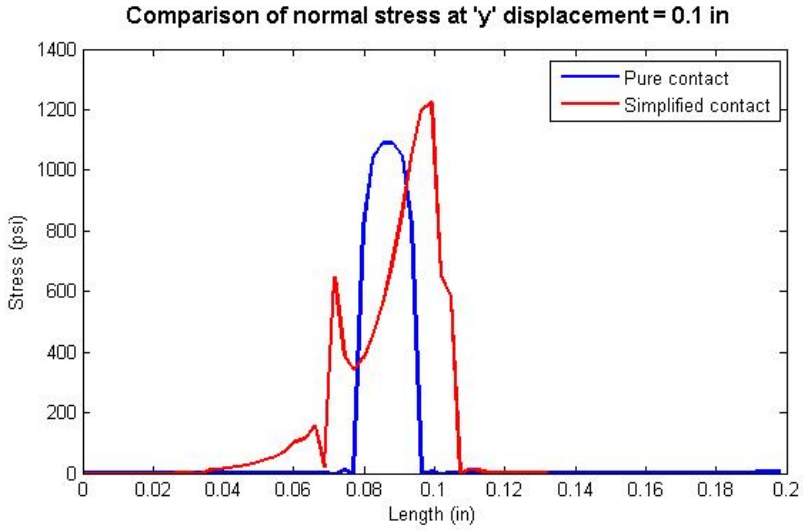

(b) At y-displacement 0.1 in

Figure 3.8.: Comparison of stress profiles along the contact surface

3.2 Bi-stable membrane mechanism for 3D persistent sliding contact

The concept of bi-stable spring mechanism is extended to three-dimensional problems using membrane elements as shown in Figure 3.9. The simplified contact model

in this case consists of devices made from a membrane that serves the same purpose as that of the spring in 2D, and a wall that, similar to the cross elements in 2D, provides the supporting structure for the membrane. The membrane is a thin sheet-like structure which is stiff in tension, but has no resistance to compression. The bistable configuration of the membrane beam is used to achieve the desired sliding contact behavior in 3D models.

3.2.1 Behavior of the bi-stable wall-membrane model

This model consists of two parallel walls connected by a thin membrane as shown in Figure 3.9. Shell elements are selected for membrane and solid elements for walls. Along the edge where the membrane meets the wall, only translational degrees of freedom are coupled so that the connection acts as a hinge and allows flipping of the membrane. As shown in Figure 3.9, the top and bottom faces of the left wall are fixed and a vertical displacement is provided to the top and bottom faces of the right wall.

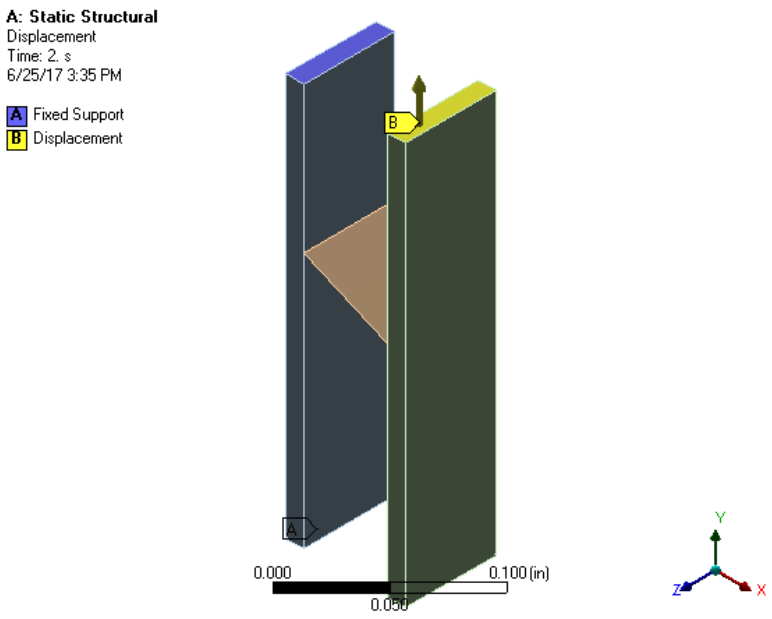

Figure 3.9.: Parallel wall model

As expected, the membrane exhibits bi-stable configurations similar to the bi-stable spring elements. It is in a stress-free in the initial and final flipped configurations and has the maximum stress when the membrane is horizontal. Figure 3.10 show the three positions of the membrane thus validating the concept. The force deformation plots for this mechanism are shown in Figure 3.11 and are obtained from reaction forces in the x, y and z directions at the fixed support and displacement ends of the walls. Figure 3.11(h) shows that only a small vertical force is needed to flip the membrane between its two stable stress-free configurations A and B. Beyond points A and B, there is resistance to the movement in the y-direction as the membrane comes into tension and this corresponds to the limits of the sliding movement between the contacting surfaces. Figure 3.11(g) shows that forces in the x-direction are much larger so as to resist movement in the x-direction

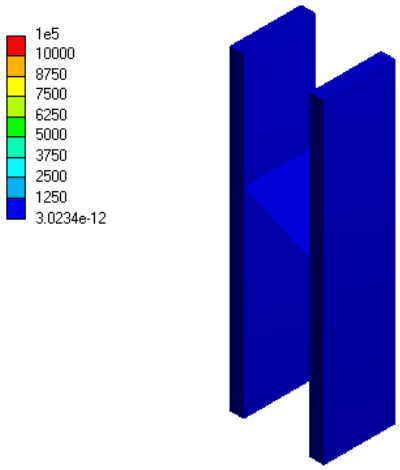

(a) initial state

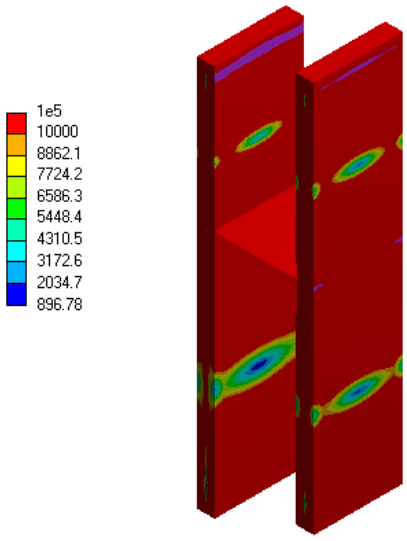

(b) maximum stress position

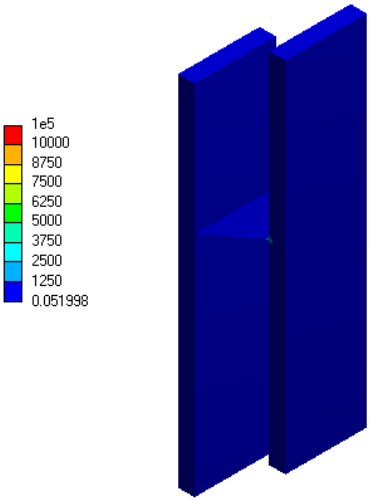

(c) final flipped state

Figure 3.10.: Bi-stable configurations of the wall and membrane device

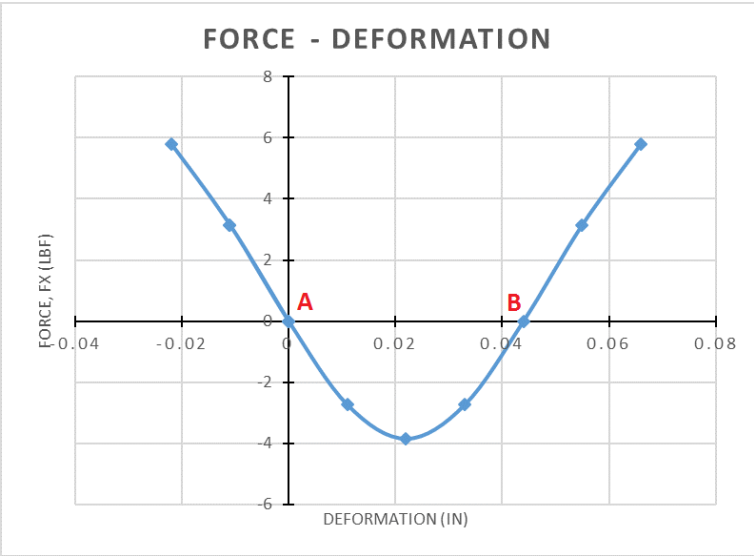

(a) Parallel wall-forces in x-direction

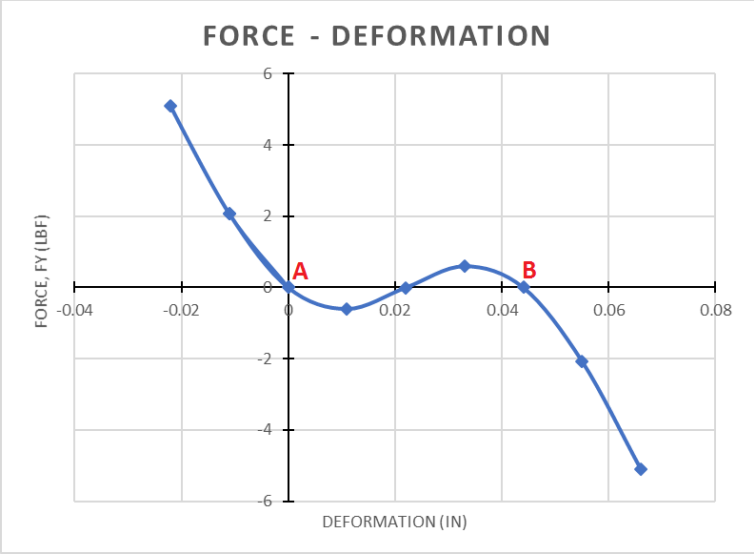

(b) Parallel wall-forces in y-direction

Figure 3.11.: Force-deformation plots for the bi-stable wall and membrane device

3.2.2 Sliding contact of two cantilever beams in 3D

The two cantilever beams 2D model explained earlier is developed in 3D. The geometry is as shown in Figure 3.12. The vertical (y) displacement is provided to the

far end faces of the cantilever beams in opposite directions as shown in Figure 3.12. The cantilever beams slide and separate from each other. This model is tested to know the range of vertical displacement the simplified model can bear. The details of the model are provided in Table 3.3.

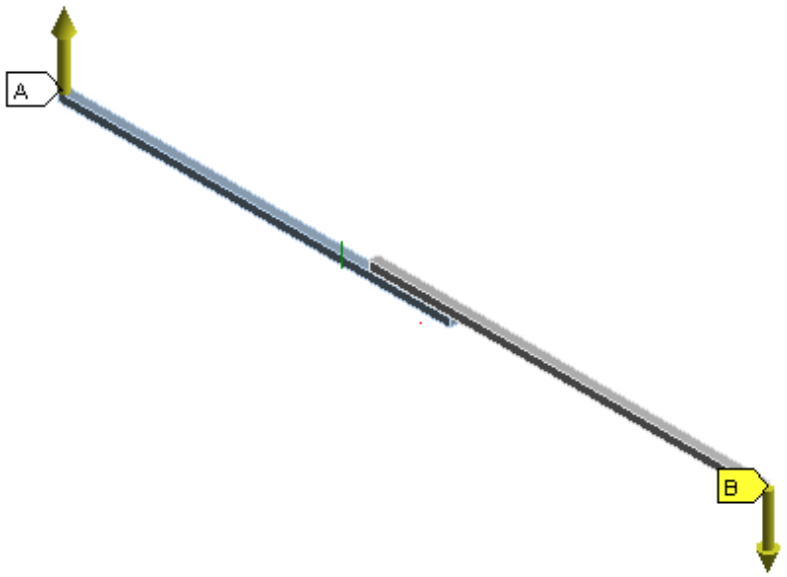

Figure 3.12.: Cantilever 3D model

The wall-membrane device is used to develop the simplified contact model instead of spring-cross element device. The arrangement of wall-membrane device is shown in 3.13(i). The full simplified model is shown in Figure 3.13(j). Wall 'A' is attached to the upper cantilever beam to reproduce contact stresses and wall 'B' to the lower beam. A membrane 'C' is connected to the two walls as a hinge hence facilitating flipping of the membrane which in turn allows sliding and avoids penetration.

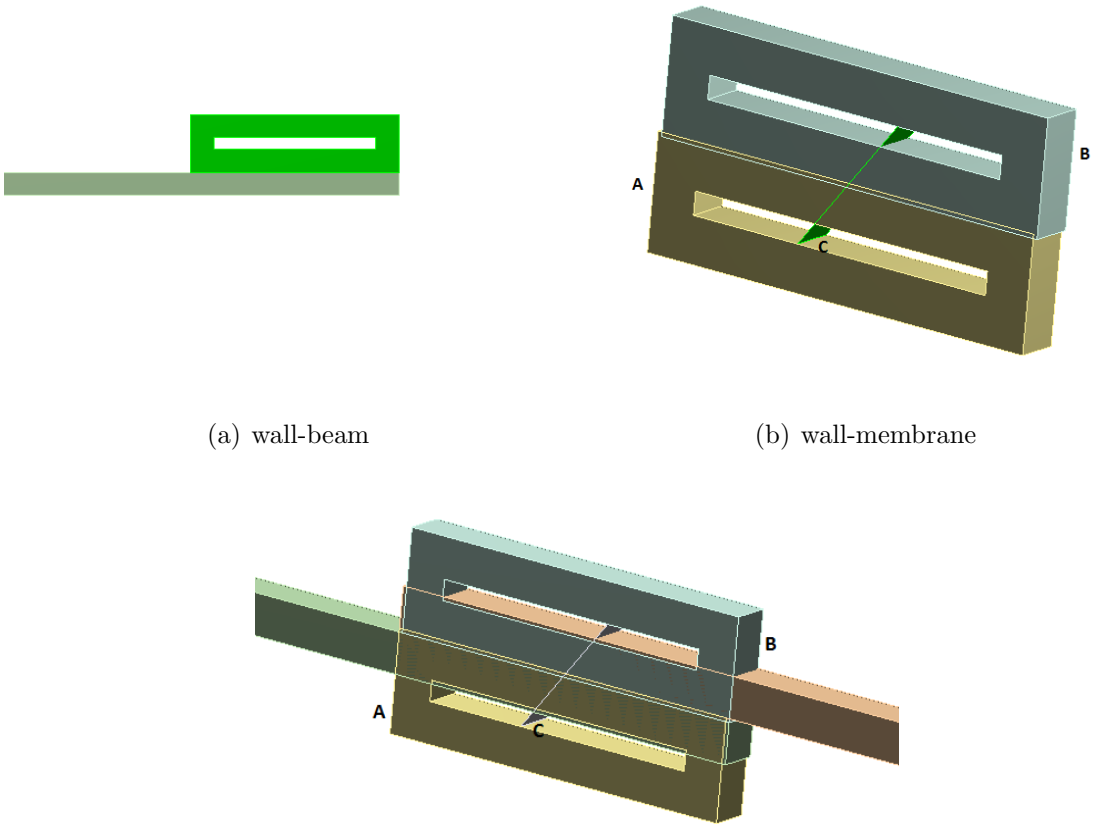

(a) wall-beam

(b) wall-membrane

(c) wall-membrane attached to beams

Figure 3.13.: Simplified contact model in 3D using a wall-membrane device

Table 3.3.: Properties of cantilever beam 3D model

Geometrical dimensions		Lower beam	Upper beam	
	Length X	0.485 in.	0.485 in.	
	Length Y	0.011 in.	0.011 in.	
	Length Z	0.011 in.	0.011 in.	
Material properties (Cantilever Beams)	Material	Structural steel		
	Youngs modulus	2.9E+07 psi		
	Poissons ratio	0.3		
	Behavior	Isotropic elastic		
Contact	Frictionless			
Mesh	Method	Hex dominant		
	Element Size	0.00275 in		
	Nodes	8900		
	Elements	5664		
Boundary conditions	Displacement(in)	X	Y	Z
	Edge A	0	-0.1 in	0
	Edge B	0	0.1 in	0

Minimum principal stress graphs are plotted for both the models to calibrate the simplified model to the contact model. The top view of lower cantilever beam is shown in Figure 3.14. Three lines of nodes are considered marked as 1, 2 and 3 in Figure 3.14. The nodes start from point 'O' and end at point 'P'. The length is measured from point 'O' to 'P'.

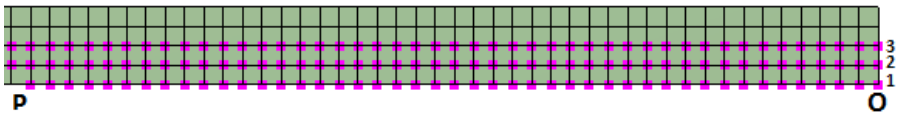

Figure 3.14.: Top view of lower cantilever beam

The stress is calculated at each node and plotted on y-axis with length on x-axis. For each model, three stress plots are developed corresponding to three lines of nodes. Different cases are considered as shown in Figure 3.4 by varying the stiffness of walls, membrane, angle between the walls and membrane, geometrical dimensions of walls and membrane. Figure 3.15, Figure 3.16, Figure 3.17 show the comparison of variation of stress along the considered nodal lines(L1, L2, L3) between the contact and the simplified model. The comparison of the deformed shapes of the cantilever beams is shown in Figure 3.18 and Figure 3.19 . The 3D cantilever beam pure contact model was converged in 12 - 13 hours whereas the corresponding simplified model in about 2 hours.

Table 3.4.: cases considered

Case no.	Stiffness of membrane(psi)	Stiffness of walls / stiffness of beams	Mesh size(in)
1	2.90E+05	10^1	0.00275
2	2.90E+07	10^1	0.00275
3	2.90E+05	10^2	0.00275
4	2.90E+06	10^1	0.00275
5	2.90E+04	10^3	0.00275

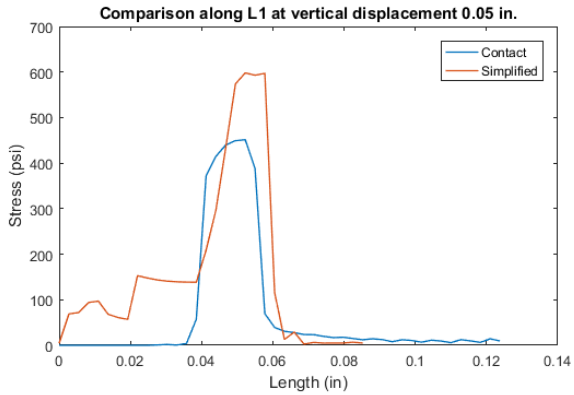

(a) Along Line 1 at 0.05 in

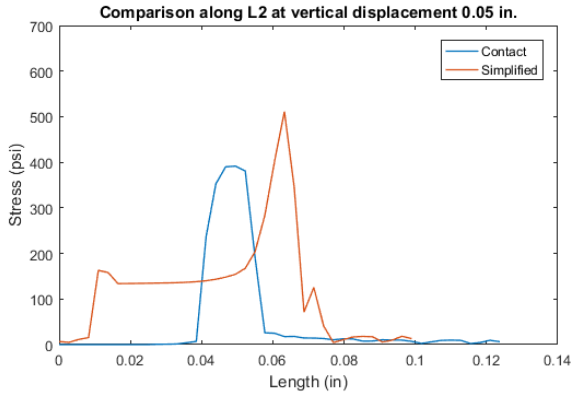

(b) Along Line 2 at 0.05 in

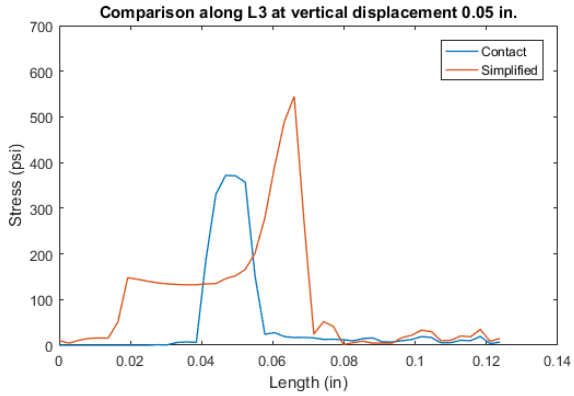

(c) Along Line 3 at 0.05 in

Figure 3.15.: Cantilever 3D comparison plots at 0.05 in

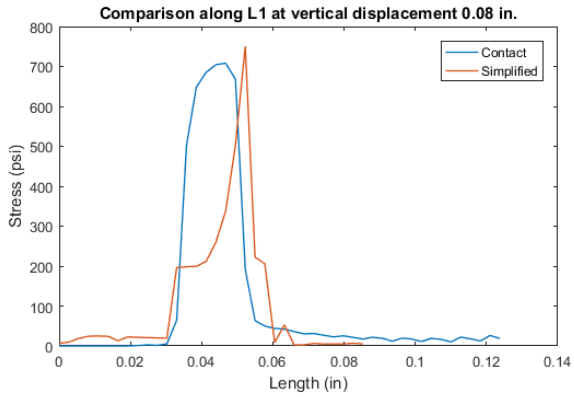

(a) Along Line 1 at 0.08 in

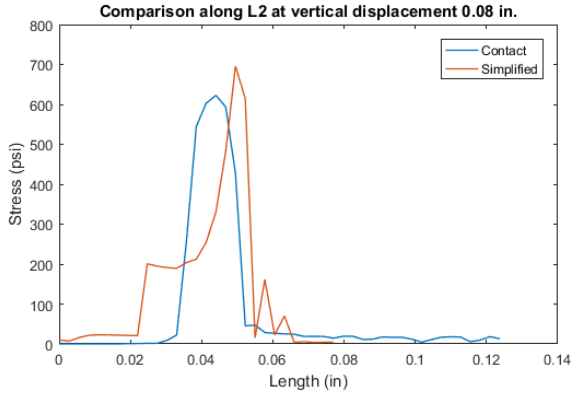

(b) Along Line 2 at 0.08 in

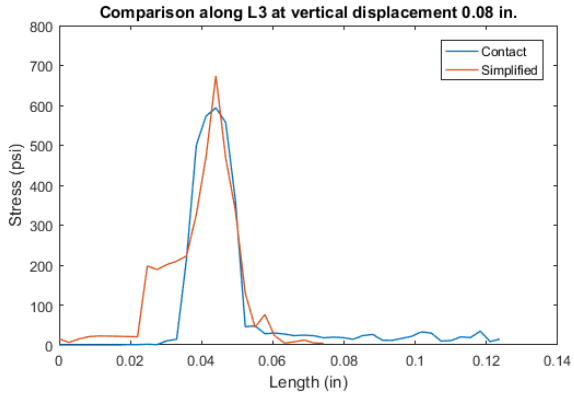

(c) Along Line 3 at 0.08 in

Figure 3.16.: Cantilever 3D comparison plots at 0.08 in

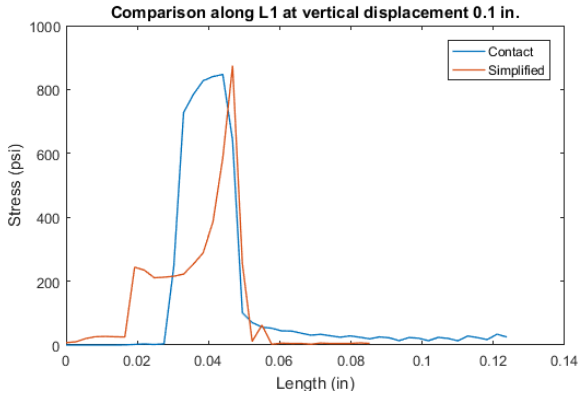

(a) Along Line 1 at 0.1 in

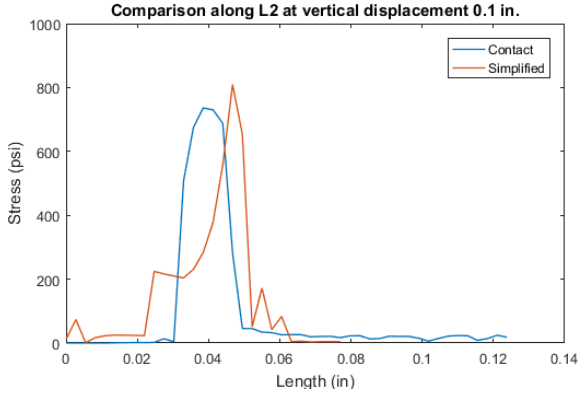

(b) Along Line 2 at 0.1 in

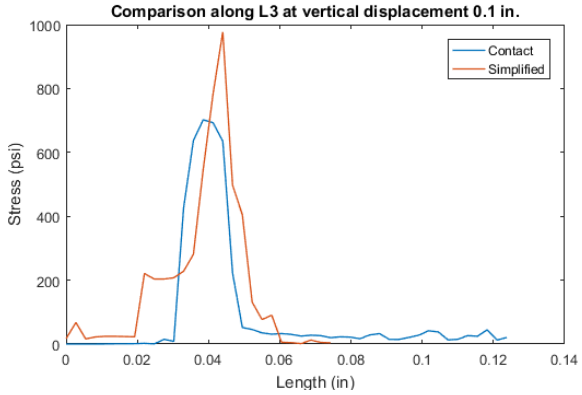

(c) Along Line 3 at 0.1 in

Figure 3.17.: Cantilever 3D comparison plots at 0.1 in

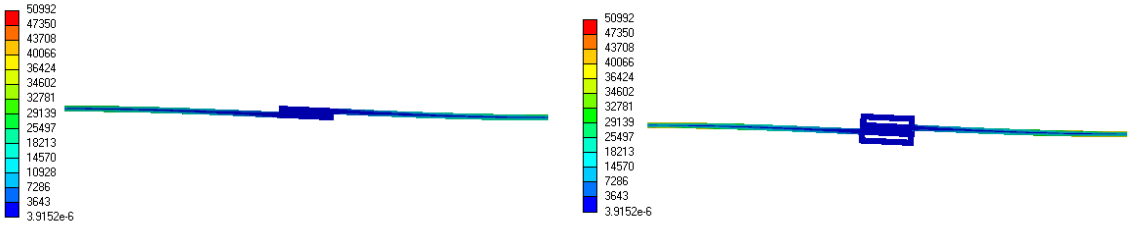

(a) contact model at initial state (b) simplified model at initial state

Figure 3.18.: Deformed shapes at initial state

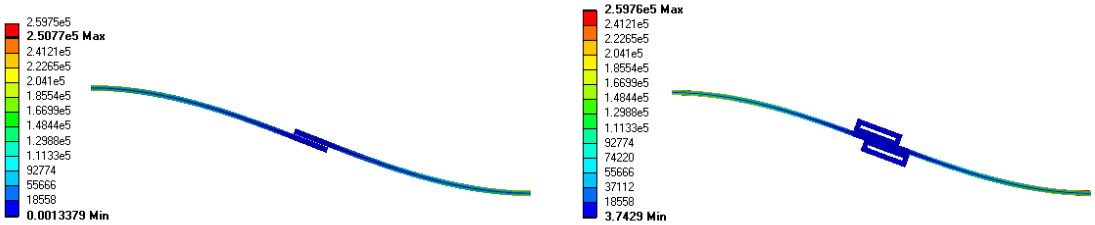

(a) contact model at final state (b) simplified model at final state

Figure 3.19.: Deformed shapes at flipped state

As mentioned, the calibration of the simplified model depends on stiffness of walls, membrane, angle between the walls and membrane, geometrical dimensions of walls and membrane. Higher accuracy can be obtained by simulating more trials by developing further combination of the parameters mentioned.

3.3 Sliding contact between two concentric rings

Concentric ring model is a simpler version of two ring interlock model. As mentioned earlier the cross-section of the interlock consists of two S-shaped rings arranged to form a lock. The concentric ring model consists of two circular cross-sections overlapping by a certain amount. These cross-sections are revolved to form 3D concentric

rings. The geometrical dimensions of the concentric rings is similar to the interlock rings. The amount of play between the interlock rings is the overlap in the concentric rings. Figure 3.20 shows the geometry of the concentric rings. For comparison of the pure contact model and the simplified contact model, pure shear mode is simulated. Both the contact and simplified model are developed and compared. Each of the models are explained below.

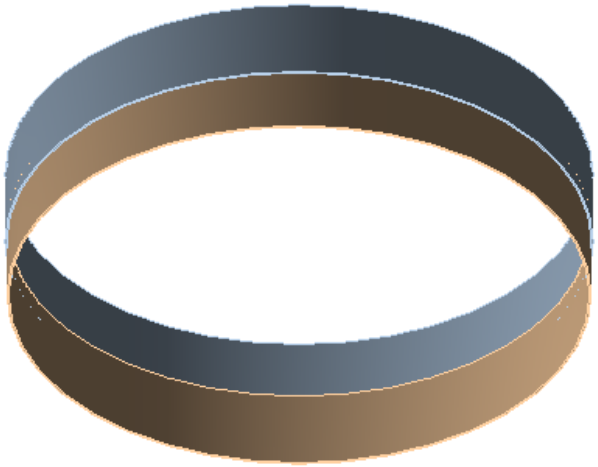

Figure 3.20.: Concentric ring

The wall-membrane approach is used to develop the simplified model. Since it is a circular body and contact is present between the two concentric rings in a circular pattern, we need the wall-membrane devices also to be circular. The parallel wall model is revolved to form a circular wall model. Boundary conditions similar to the parallel wall model are applied. As expected, the membrane achieves bi-stable configuration in circular models as well. The amount of flip the membrane undergoes is equal to the play between the interlocks or the overlap between the concentric ring models.

3.3.1 Simple shear of two concentric rings

The contact model is shown in Figure 3.21. Contact is present between the faces marked red and blue. The bottom face 'A' of the bottom ring is fixed. The displacement is provided to the top face 'B' of the top ring as shown in Figure 3.22. The properties of the contact model are provided in Table 3.5. The contact status provided by ANSYS is shown in 3.23.

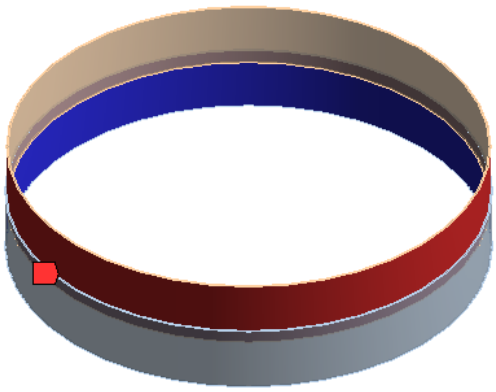

Figure 3.21.: Contact in concentric ring

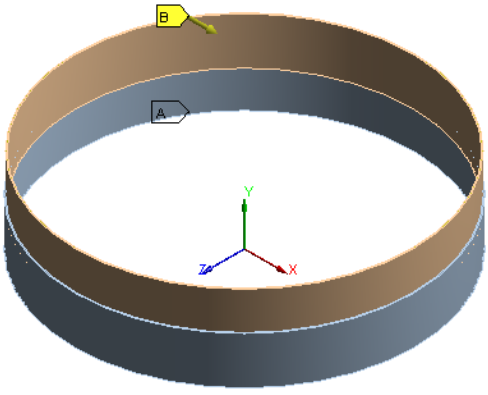

Figure 3.22.: Boundary conditions

Table 3.5.: Properties of concentric ring contact model.

Outer ring		Inner ring	
Outer radius	1.75 in	Outer radius	1.738 in
thickness	0.011 in	thickness	0.011 in
height	0.485 in	height	0.485 in
Material	In-Mac AISI 321 NL	Material	In-Mac AISI 321 NL
Youngs modulus	2.8E+07 psi	Youngs modulus	2.8E+07 psi
Contact length		0.1 in	
Initial gap		0.001 in	

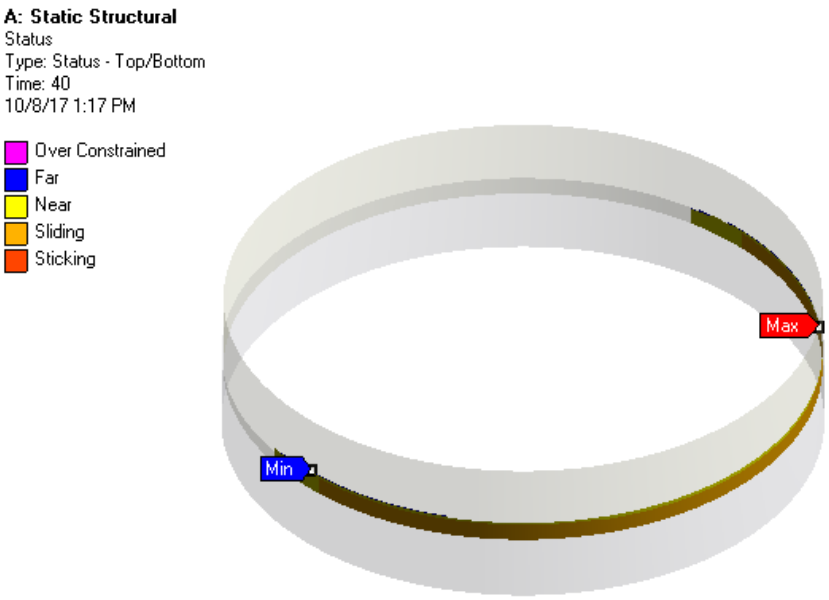

Figure 3.23.: Contact status

3.3.2 Concentric ring simplified model

The simplified concentric ring model is developed as explained earlier using wall-membrane device. The arrangement of circular walls-membrane and the concentric

rings is shown in Figure 3.24. The boundary conditions are similar to the contact model. The properties of the model are provided in Table 3.6.

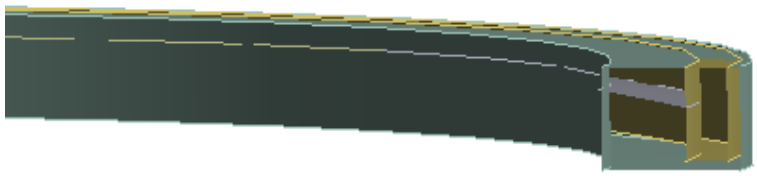

(a) circular wall

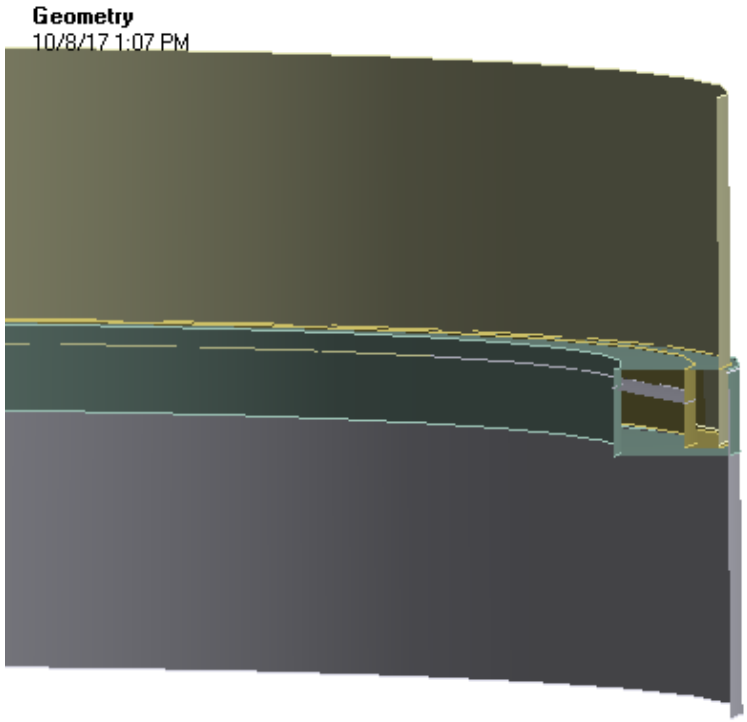

(b) Simplified concentric ring

Figure 3.24.: Concentric ring simplified contact model geometry

Table 3.6.: Properties of simplified concentric ring model

Geometry		Inner ring	Outer ring	
	Outer radius	1.738 in.	1.75 in.	
	Height	0.485 in.	0.485 in.	
	Thickness	0.011 in.	0.011 in.	
Material properties (concentric rings)	Material	In-Mac AISI 321 NL		
	Youngs modulus	2.9E+07 psi		
	Poissons ratio	0.3		
Material properties (wall elements)	Material	In-Mac AISI 321 NL 2		
	Youngs modulus	2.9E+08 psi		
	Poissons ratio	0.3		
Material properties (membrane)	Material	In-Mac AISI 321 NL 3		
	Youngs modulus	2.9E+05 psi		
	Poissons ratio	0.3		
Mesh	Method	Multi zone		
	Element size	0.011 in		
	Elements	52000		
Boundary conditions	Displacement	X	Y	Z
		0.007 in	0 in	0

Simplified models for concentric ring and two ring interlock models are developed using SHELL181 elements in ANSYS. SHELL181 is a four node element with six degrees of freedom at each node: translations in and about x, y and z directions. This element type can be used in analyzing thin to moderately thick structures, more applicable for linear, large rotation and large strain nonlinear problems. [sharcnet.com] The thickness of the element is assumed to vary smoothly over the area of the element. Figure 3.25 shows the geometry, node locations, and the element coordinate system for this element. The element is defined by shell section information and by four nodes (I, J, K, and L).

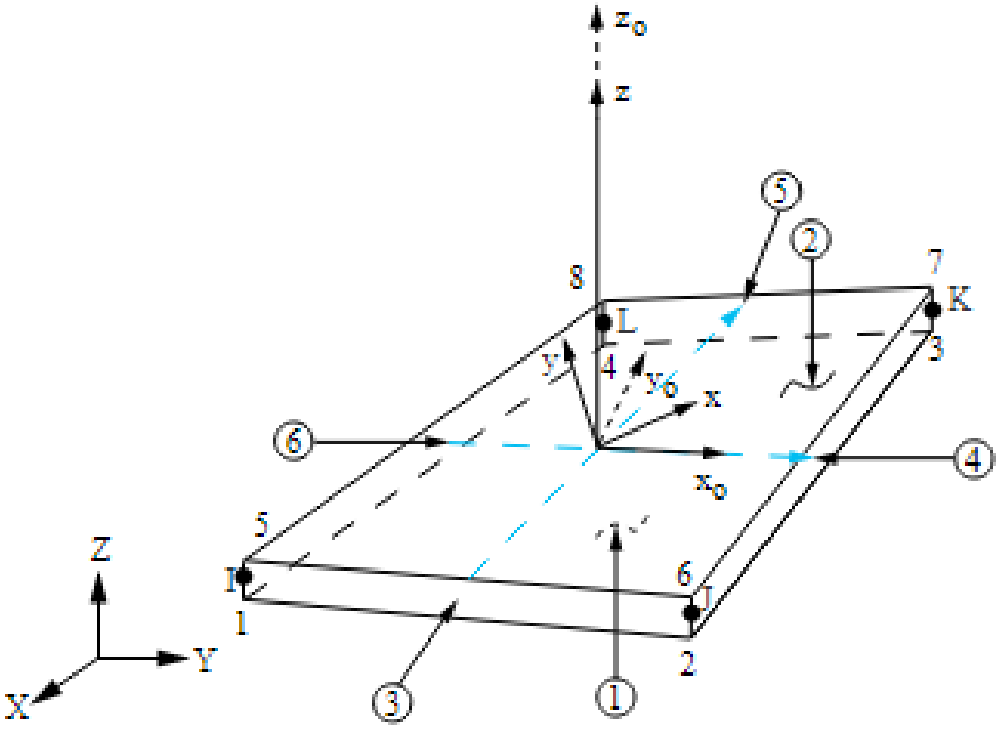

Figure 3.25.: SHELL181 (Source - ANSYS Manual)

Equivalent stress, minimum principal stress and maximum principal stress plots developed by ANSYS are considered directly for comparison between contact and simplified model. Different cases are simulated by varying the stiffness, geometrical dimensions of the wall-membrane device. The included stress plots are only for that particular case whose properties are given in Table 3.6 which was more accurate than the others. Figure 3.26 shows the comparison of Von-Mises stress plots between the concentric ring contact and simplified models. Figure 3.27 shows the normal stress plots. The concentric ring pure contact model with 32000 elements was converged in about 22-23 hours whereas the corresponding simplified model with 52000 elements in about 5-6 hours.

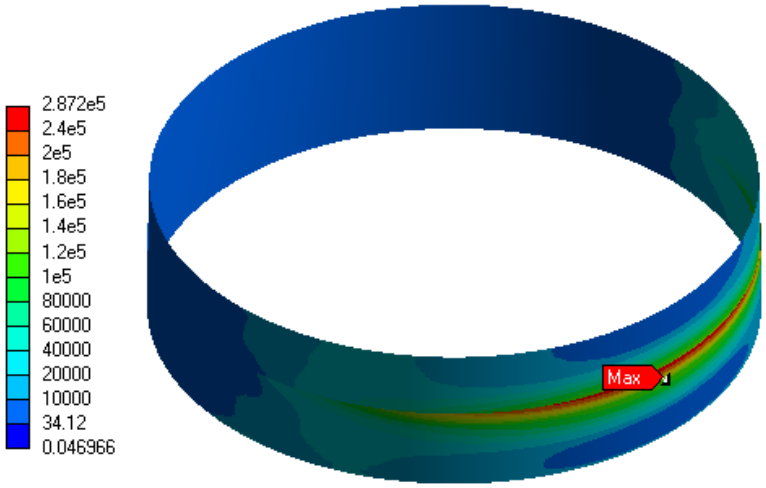

(a) Equivalent stress - concentric ring contact

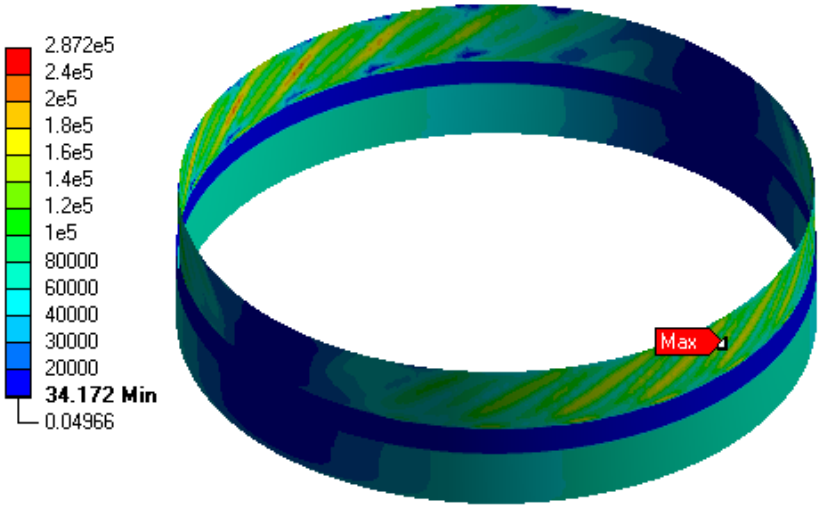

(b) Equivalent stress - concentric ring simplified

Figure 3.26.: Comparison of contact and simplified model for concentric rings - Equivalent Stress

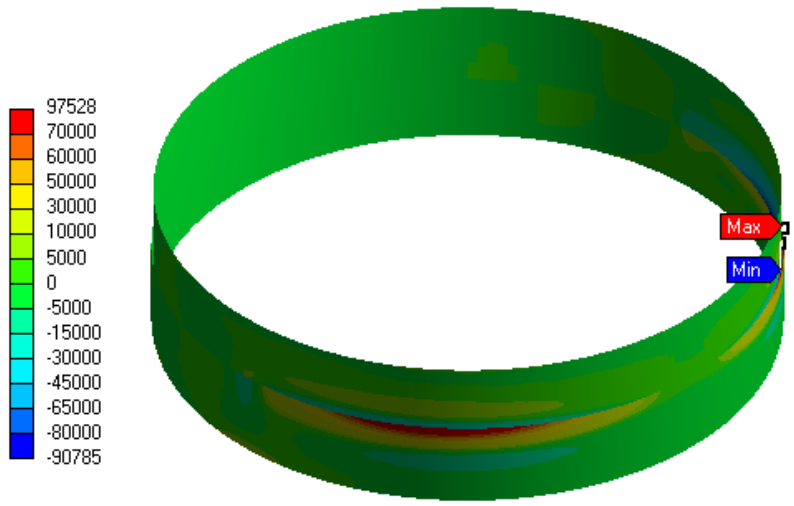

(a) Normal stress - concentric ring contact

(b) Normal stress - concentric ring simplified

Figure 3.27.: Comparison of contact and simplified model for concentric rings - Normal Stress

The accuracy of the simplified model depends on the geometrical properties and stiffness of the wall-membrane device. Once the simplified model for concentric rings

was developed and validated, the concept was extended to the interlock two ring model as explained in the following sections.

3.4 Sliding contact in a two-ring 3D interlock model

The interlock two ring 3D model is developed by rotating the cross section of interlock as explained in section 1.3. The physical set up of concentric ring model is developed using interlock two ring 3D model. The boundary conditions remain the same. The geometry and boundary conditions of the model are show in Figure 3.28. Similar to earlier, pure shear mode is considered to compare the contact and simplified models.

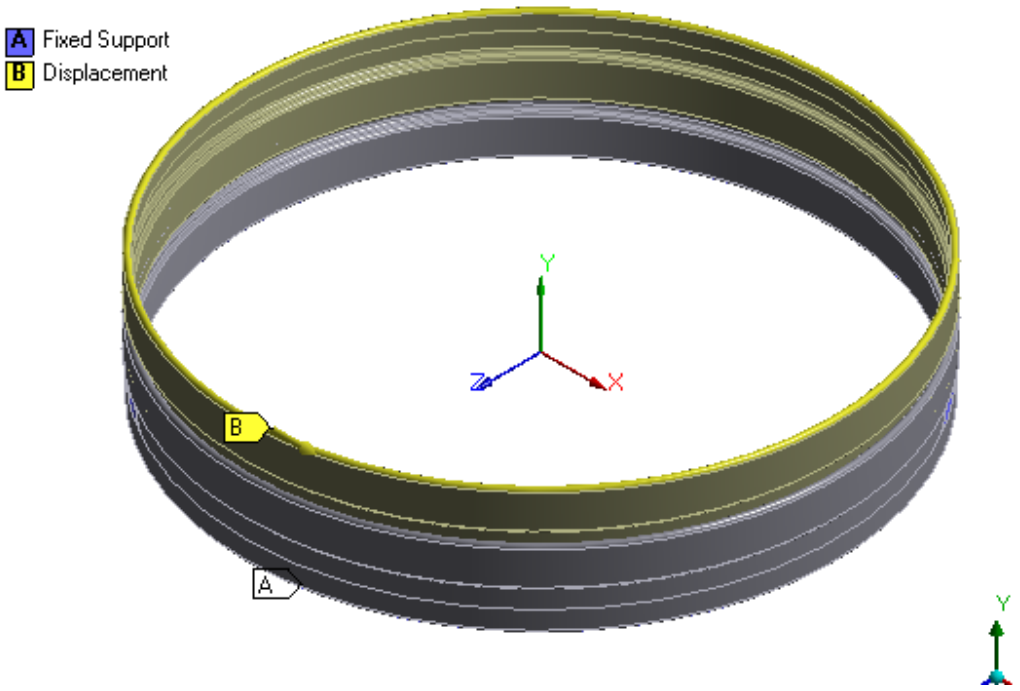

Figure 3.28.: Interlock Boundary conditions

3.4.1 Contact model

Frictionless contact is considered between the interlock ring surfaces. As explained in section 1.3, only contact surface 1 is activated. In the 3D model, the contact area is in a circular pattern as shown in Figure 3.29. SOLID186 elements are used for interlock and concentric ring contact models. It is a 3D 20 node element that exhibits quadratic displacement behavior. It has three degrees of freedom per node: translations in x, y and z directions.

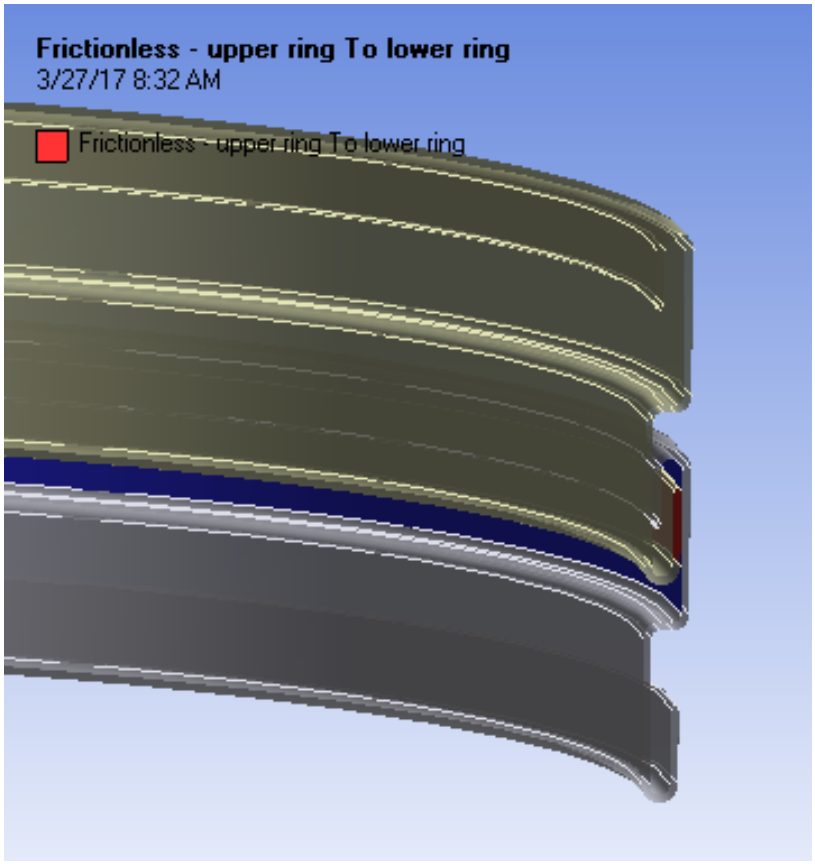

Figure 3.29.: Interlock contact

The contact status provided by ANSYS is shown in Figure 3.30

Figure 3.30.: Interlock contact status

Table 3.7.: Properties of interlock contact model

Material properties		Lower ring		Upper ring
	Material	In-Mac AISI 321 NL		
	Youngs modulus	2.8E+07 psi		
	Poissons ratio	0.3		
Contact	Frictionless			
Mesh	Method	Hex dominant		
	Element size	0.011 in		
	Elements	50400		
Boundary conditions	Displacement	X	Y	Z
		0.009 in	0 in.	0

3.4.2 Simplified model

The simplified contact model for interlocks is developed in a similar fashion as in concentric ring model. Initially, the wall-membrane device is modeled and then

attached to the two ring interlocks at the considered contact surface. The properties of the simplified model are given in Table 3.8.

Table 3.8.: Properties of simplified interlock two ring model

Geometry		Inner ring	Outer ring	
	Outer radius	1.738 in.	1.75 in.	
	Height	0.485 in.	0.485 in.	
	Thickness	0.011 in.	0.011 in.	
Material properties (interlock rings)	Material	In-Mac AISI 321 NL		
	Youngs modulus	2.9E+07 psi		
	Poissons ratio	0.3		
Material properties (wall elements)	Material	In-Mac AISI 321 NL 2		
	Youngs modulus	2.9E+09 psi		
	Poissons ratio	0.3		
Material properties (membrane)	Material	In-Mac AISI 321 NL 3		
	Youngs modulus	2.9E+06 psi		
	Poissons ratio	0.3		
Mesh	Method	Multizone		
	Element size	0.011 in		
	Elements	63800		
Boundary conditions	Displacement	X	Y	Z
		0.009 in	0 in	0

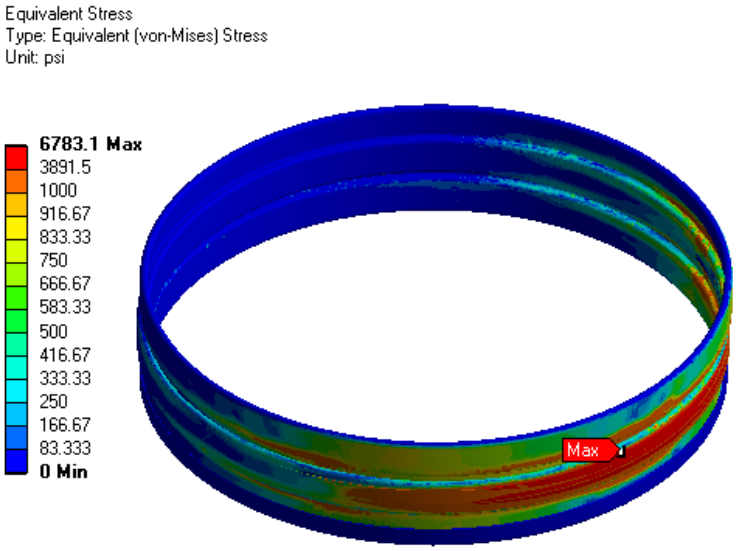

(a) Equivalent stress - interlock contact

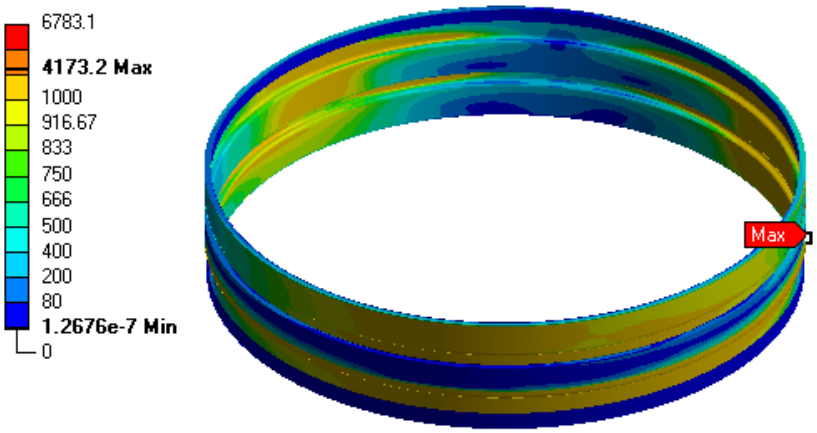

(b) Equivalent stress - interlock simplified

Figure 3.31.: Comparison of contact and simplified model for interlock two ring model - Equivalent stress

(a) Maximum principal stress - interlock contact

(b) Maximum principal stress - interlock simplified

Figure 3.32.: Comparison of contact and simplified model for interlock two ring model - Maximum principal stress

3.4.3 Results and Comparison

Comparison between the pure contact and simplified contact models is done by plotting equivalent stress plots as shown Figure 3.31, maximum principal stress plots as shown in Figure 3.32. The time taken to converge by the contact model with 50400 elements was approximately 25 hours whereas the time taken by the simplified model with 63800 elements was around 7-8 hours. The simulation time has reduced drastically which reduces the computational expenditure however it's difficult to reproduce the exact amount and location of stresses similar to the pure contact model. Given that it's a simplified approach, it loses some accuracy in the solution.

4. CONCLUSIONS AND FINDINGS

Contact problems are very difficult to solve even using the state of the art commercial software programs. Depending upon loading and boundary conditions, contact regions are constantly evolving between bodies and this makes it a highly non-linear problem. Due to this, contact problems solved in this research were computationally very expensive and often consumed hours or days for the bigger models to simulate. Despite making all the contact models in this document frictionless, there were lot of convergence issues with these models. Over the course of the research, it was observed that the simplified contact models reduced the simulation time of contact problems drastically while providing results that matched well in comparison to pure contact models. This is a significant computational advantage of the simplified contact models.

While the overall response of the contacting bodies was represented well by simplified contact models, some differences were observed in the region of actual contact and the precise value of the contact stresses. Accuracy of the simplified models depends on geometrical dimensions, material properties, stiffness of the simplified devices such as wall-membrane, cross elements, and the spring elements. Greater accuracy in the results can be achieved by further exploring these parameters.

4.1 Recommendations for future studies

Performance of the simplified contact models developed in this research mainly depends on the geometrical dimensions and the material properties of the various elements. In future, studies may be undertaken to improve the contact stress profile obtained in the simplified models. This may be accomplished potentially by adaptively modifying the geometry and material properties of the supporting structures

(cross elements and wall elements) and the spring or membrane elements. Adapting these simplified contact devices to contact problems that involve different types elements, such as continuum and/or structural elements may also be worth exploring.

REFERENCES

REFERENCES

[1] K. Johnson, "Contact mechanics cambridge univ," *Press, Cambridge*, 1985.

[2] C. L. Brockett, P. Harper, S. Williams, G. H. Isaac, R. S. Dwyer-Joyce, Z. Jin, and J. Fisher, "The influence of clearance on friction, lubrication and squeaking in large diameter metal-on-metal hip replacements," *Journal of Materials Science: Materials in Medicine*, vol. 19, no. 4, pp. 1575–1579, 2008.

[3] F. Bucher and R. Dwyer-Joyce, "The real area of contacta combination of experimental and numerical approaches," in *Contact Mechanics*. Springer, 2002, pp. 219–228.

[4] V. A. Yastrebov, "Introduction to computational contact mechanics," *WEMESURF short course on contact mechanics and tribology*, 2010.

[5] V. L. Popov, R. Pohrt, and M. Heß, "General procedure for solution of contact problems under dynamic normal and tangential loading based on the known solution of normal contact problem," *The Journal of Strain Analysis for Engineering Design*, vol. 51, no. 4, pp. 247–255, 2016.

[6] E. N. McGruer and G. G. Adams, "www.ece.neu.edu/edsnu/mcgruer /class/mems/contactmechanics1010.ppt."

[7] J. Greenwood and J. P. Williamson, "Contact of nominally flat surfaces," in *Proceedings of the Royal Society of London A: Mathematical, Physical and Engineering Sciences*, vol. 295, no. 1442. The Royal Society, 1966, pp. 300–319.

[8] R. S. Bradley, "Lxxix. the cohesive force between solid surfaces and the surface energy of solids," *The London, Edinburgh, and Dublin Philosophical Magazine and Journal of Science*, vol. 13, no. 86, pp. 853–862, 1932.

[9] B. Derjaguin, "Colloid interface sci. 1975, 53, 314. muller, vm; derjaguin, bv; toporov, yu. p," *Colloids Surf*, vol. 7, p. 251, 1983.

[10] D. Maugis, "On the contact and adhesion of rough surfaces," *Journal of adhesion science and technology*, vol. 10, no. 2, pp. 161–175, 1996.

[11] S. Alliney, A. Tralli, and C. Alessandri, "Boundary variational formulations and numerical solution techniques for unilateral contact problems," *Computational Mechanics*, vol. 6, no. 4, pp. 247–257, 1990.

[12] R. Glowinski, J.-L. Lions, R. Trémolières, and J.-L. Lions, *Numerical analysis of variational inequalities*. North-Holland Amsterdam, 1981, vol. 8.

[13] P. Wriggers, *Computational contact mechanics*. Springer Science & Business Media, 2006.

[14] B. Brogliato and B. Brogliato, *Nonsmooth mechanics*. Springer, 1999.

[15] T. Wanheim, N. Bay, and A. Petersen, "A theoretically determined model for friction in metal working processes," *Wear*, vol. 28, no. 2, pp. 251–258, 1974.

[16] B. Avitzur and Y. Nakamura, "Analytical determination of friction resistance as a function of normal load and geometry of surface irregularities," *Wear*, vol. 107, no. 4, pp. 367–383, 1986.

[17] L. Anand, "A constitutive model for interface friction," *Computational Mechanics*, vol. 12, no. 4, pp. 197–213, 1993.

[18] S. Stupkiewicz, "Extension of the node-to-segment contact element for surface-expansion-dependent contact laws," *International Journal for Numerical Methods in Engineering*, vol. 50, no. 3, pp. 739–759, 2001.

[19] Z. Mroz and S. Supkiewics, "Constitutive modelling of slip and wear in elastic, frictional contact., pro. contact mechanics int. symp., edir. a," *Curnier. PPUR*, pp. 133–156, 1992.

[20] N. Kikuchi and J. T. Oden, *Contact problems in elasticity: a study of variational inequalities and finite element methods*. SIAM, 1988.

[21] M. Cocu, "Existence of solutions of signorini problems with friction," *International journal of engineering science*, vol. 22, no. 5, pp. 567–575, 1984.

[22] P. Rabier, J. Martins, J. Oden, and L. Campos, "Existence and local uniqueness of solutions to contact problems in elasticity with nonlinear friction laws," *International Journal of Engineering Science*, vol. 24, no. 11, pp. 1755–1768, 1986.